LysM-RLK plays an ancestral symbiotic function in plants

Eve Teyssier[1], Sabine Grat[1], David Landry[2], Mathilde Ouradou[1], Mélanie K. Rich[1], Sébastien Fort[3], Jean Keller[1], Benoit Lefebvre[2], Pierre-Marc Delaux[1]*, Malick Mbengue[1]*

1. Laboratoire de Recherche en Sciences Végétales (LRSV), Université de Toulouse, CNRS, UPS, INP Toulouse, Castanet-Tolosan, France.

2. Laboratoire des Interactions Plantes-Microbes-Environnement (LIPME), Université de Toulouse, INRAE, CNRS, Castanet-Tolosan, France.

3. Univ. Grenoble Alpes, CNRS, CERMAV, 38000 Grenoble, France.

*Correspondence:

pierre-marc.delaux@cnrs.fr

malick.mbengue@univ-tlse3.fr

Abstract

Arbuscular mycorrhiza (AM) with soilborne Glomeromycota fungi was pivotal in the conquest of land by plants almost half a billion years ago. In flowering plants, it is hypothesised that AM is initiated by the perception of AM-fungi-derived chito- and lipochito-oligosaccharides (COs/LCOs) in the host via Lysin Motif Receptor-Like Kinases (LysM-RLKs). However, it remains uncertain whether plant perception of these molecules is a prerequisite for AM establishment and for its origin. Here, we made use of the reduced LysM-RLK complement present in the liverwort *Marchantia paleacea* to assess the conservation of the role played by this class of receptors during AM and in COs/LCOs perception. Our reverse genetic approach demonstrates the critical function of a single LysM-RLK, LYKa, in AM formation, thereby supporting an ancestral function for this receptor in symbiosis. Binding studies, cytosolic calcium variation recordings and genome-wide transcriptomics indicate that another LysM-RLK of *M. paleacea*, LYR, is also required for triggering a response to COs/LCOs, despite being dispensable for AM formation. Collectively, our results demonstrate that the perception of symbionts by LysM-RLK is an ancestral feature in land plants, and suggest the existence of yet-uncharacterised AM-fungi signals.

Introduction

To ensure their water and mineral nutrition, most land plants form arbuscular mycorrhiza (AM) with soil-borne Glomeromycota fungi [1]. This ~450 million years old symbiosis was key in driving land colonisation by plants [2]. In angiosperms, AM is thought to be initiated via the perception by the host plant of AM-fungi derived chito- (COs) and lipochito-oligosaccharides (LCOs) leading to the activation of a conserved signalling pathway referred to as the Common Symbiosis Signalling Pathway (CSSP) [3]. Mutation of any CSSP gene, such as the receptor-like kinase *SYMRK* [4], leads to the inability to associate with AM-fungi in species as diverse as legumes [4,5], monocots [6,7] or bryophytes [8,9].

Genetics in legumes and monocots have demonstrated that members of the diversified Lysin motif Receptor-Like Kinase (LysM-RLK) family, which encompasses up to 22 members in legumes [10], are important for the perception of these AM-fungi derived molecules [11,12]. Only one double mutant in the legumes *Medicago truncatula* and *Lotus japonicus* showed a phenotype phenocopying mutants of the CSSP with a total lack of colonisation, demonstrating the importance of this family of receptors for AM in flowering plants [13,14]. However, none of the mutant combinations fully abolished the perception of both COs and LCOs, thus not allowing to determine whether these symbiotic signals are sufficient for AM establishment or whether other signal(s) are involved. The LysM-RLK family expansion that occurred in angiosperms likely complicate such analysis due to genetic redundancy.

Angiosperms, such as legumes and monocots, belong to the vascular plants. The other group of land plants, the bryophytes, includes species with a haploid-dominant life-cycle such as the liverwort *Marchantia paleacea*. Because the bryophyte and vascular plant lineages diverged from each other soon after the colonisation of lands by plants, any trait found to be conserved in both clades can be inferred as ancestral in plants [15,16]. Using reverse genetics in *M. paleacea* and comparison with vascular plants, it has been demonstrated that AM has been relying on lipids provided by the host plants for 450 million years [17]. Furthermore, mutations in any of the CSSP gene in *M. paleacea* lead to the total absence of colonization by AM fungi, as observed in angiosperms [8,9]. It can thus be hypothesised that at least part of the signalling processes involved in the formation of AM in *M. paleacea* and angiosperms are similar. In contrast to angiosperms, the liverwort *M. paleacea* contains only four LysM-RLKs (see below), limiting the expected genetic redundancy observed in angiosperms. *M. paleacea* therefore represents a unique model to study the role of CO- and LCOs-signalling and determine whether other signals are involved in AM establishment.

In this study, we demonstrate the essential role for AM in *M. paleacea* of a single LysM-RLK, pro-ortholog to the highly diversified CERK1 clade in most angiosperms. Moreover, we demonstrate that the ability of *M. paleacea* to respond to COs and LCOs is fully abolished in that mutant. Yet, we present genetic evidence that signalling triggered by COs and LCOs is not essential for AM in *M. paleacea*, suggesting the existence of additional and uncharacterised AM-fungi signals.

Results

Marchantia paleacea has a limited number of LysM-RLKs

Phylogenetic analyses indicate that LysM-RLK originated in streptophyte green algae and diversified following the colonisation of land by plants [18,19]. Extant liverworts harbour four clades, including three LYKs with a predicted active kinase and one LYR with a deleted activation loop in the kinase domain [20]. All LysM-RLKs of *M. paleacea* contain a predicted N-terminal signal peptide, a LysM-containing extracellular domain, a transmembrane region and an intracellular kinase domain. Based on the established nomenclature for LysM-RLKs [10], *M. paleacea* LYKa belongs to the LYK-I subclade that contains the immunity-related chitin co-receptor CERK1 from *Arabidopsis thaliana* [21] and the symbiotic Nod factor co-receptor NFR1 from *Lotus japonicus* [22] (**Fig 1**). As a unique member, MpaLYKa therefore represents the pro-ortholog in *M. paleacea* of all members of the LYK-I subclade in angiosperm. Similarly, MpaLYKb and MpaLYKc are pro-orthologous to the LYK-II and LYK-III subclades, respectively, while the single MpaLYR is pro-orthologous to the entire LYR-I to LYR-IV subclades (**Fig 1**). *Marchantia polymorpha*, that has lost the ability to form AM [23], contains only two *LYKs* and one *LYR* [20]. Remnants of a third *LYK* gene in *M. polymorpha*, encoding a truncated receptor from the LYK-II subclade, accounts for this discrepancy between Marchantia species (**Fig 1**).

Mutation of a single *LYK* gene in *Marchantia paleacea* leads to symbiosis impairment

To determine the contribution of individual LysM-RLKs from the *M. paleacea* LYK clade to AM, we generated loss-of-function mutants for *MpaLYKa*, *MpaLYKb* or *MpaLYKc*. For that, CRISPR/Cas9 was used in combination with single guide-RNAs (sgRNA) designed to target the 5' region of the genes, hereby breaking the link between the signal peptide and the remaining part of these type-I membrane proteins (**S1 Fig**). Following plant transformation and subsequent progeny selection, we recovered independent mutant lines for each *LYK* gene. Sanger sequencing of induced mutations are summarized in **S1 Table**. For *MpaLYKa* and *MpaLYKb*, only one of the two sgRNAs proved effective in inducing frameshift-causing INDELs whereas the two different sgRNAs designed against *MpaLYKc* were effective in inducing *null* mutations. For each LYK, we kept a minimum of two *null* mutant lines resulting from independent T-DNA transformation events and assessed their ability to form AM in comparison to an empty vector-containing control line. Six weeks after inoculation with spores of the AM fungus *Rhizophagus irregularis*, we evaluated the colonisation status of *M. paleacea* by histological observations of transversal (**Fig 2A-D**) or longitudinal (**S2 Fig A-D**) sections of the thallus. A strong pigmentation along the midrib of the thallus is a marker of a positive mycorrhizal colonisation in *M. paleacea* [24]. This pigmentation was visible in control, *lykb* and *lykc* mutants but absent in *lyka*, suggesting successful symbiosis establishment in *lykb* and *lykc* and a lack of fungal colonisation in *lyka*

(**Figs 2A-D and S2 A-D - middle panels**). Wheat-Germ-Agglutinin (WGA)-Alexa Fluor staining of fungal cell wall confirmed the presence of arbuscules in the thalli of control, *lykb* and *lykc* plants. In contrast, no intercellular hyphae nor arbuscules were observed in *lyka* (**Figs 2A-D and S2A-D - left and right panels**), confirming the absence of AM in these mutants. Over two large scale experiments, quantitative analysis of the exclusion zone length [2] as well as the percentages of mycorrhizal plants per genotype did not reveal differences between *lykb* or *lykc* alleles compared to the control (**Figs 2E and S2E**). In contrast, these experiments confirmed AM-defectiveness in three independent *lyka* mutants, representing approximately 300 measurements in total for this class of mutant.

To verify that the absence of fungal colonisation in *lyka* was not due to a delay in AM establishment, we harvested *lyka* ten weeks after inoculation with *R. irregularis* spores. Again, we were unable to observe accumulation of the AM-related pigment or positive WGA-Alexa Fluor signal in the thalli of inoculated *lyka* plants (**Fig 2F**). Next, we tested for complementation of *lyka* when co-cultivated in proximity to wild-type *M. paleacea* that had been hosting AM fungi for several weeks. This nurse-plant method has been successfully used to distinguish between defaults in penetration and in survival of AM fungi in mutants. Six weeks after the start of the co-culture with nurse plants, the empty-vector control plants showed an 86% success rate in fungal colonisation (**Fig 2G**). Conversely, none of the *lyka* plants grown under these conditions were colonised (**Fig 2G**), indicating that the *lyka* phenotype is not due to a secondary effect on the fungal symbiont but is rather the direct consequence of a non-functional MpaLYKa-dependent signalling pathway in the host. We therefore conclude that, within the *LYK* clade of *M. paleacea*, *MpaLYKa* is critical for AM establishment whereas *MpaLYKb* and *MpaLYKc* are dispensable.

The single LYR gene from *Marchantia paleacea* is not essential for arbuscular mycorrhiza

Contrary to AM-host angiosperms, which carry between 4 and 11 LYR paralogs [10], the genome of *M. paleacea* contains a single *LYR* gene [23] (**Fig 1**). To assess its contribution to symbiosis, we generated *lyr* loss-of-function alleles using CRISPR/Cas9 and two independent sgRNAs, as previously described (**Fig S1 and Table S1**), and tested their ability to form AM. As performed for the *lyk* mutants, we evaluated the colonisation status of the *lyr* mutants by histological observations of transversal (**Fig 3A**) or longitudinal (**Fig S3A**) sections of the thallus. We observed no differences in thallus pigmentation between empty-vector control and *lyr*, suggesting similar colonisation levels in both genotypes. WGA-staining confirmed the presence of arbuscules in both control and *lyr* lines (**Figs 3A and S3A**). Similarly to what we observed for the *lykb* and *lykc* mutants, quantitative analysis of the exclusion zone length [2] as well as the percentages of mycorrhizal plants per genotype did not point at reproducible differences between *lyr* alleles and control (**Figs 3B and S3B**). Over two large scale experiments, control plants displayed a total of 98% mycorrhizal success rate and *lyr* alleles followed closely with 92% and 96% mycorrhizal success rate. The mean lengths of the exclusion zone were

121 similar between genotypes, although a slight difference of approx. 1 mm was measured across
122 replicates (**Figs 3B and S3B**). The absence of AM phenotype in mutants of the single *LYR* gene
123 demonstrates the non-essential role for this clade of LysM-RLK for AM establishment in *M. paleacea*.

124 MpaLYR is the COs/LCOs receptor of *Marchantia paleacea*

125 In order to gain insights into the functional roles of *M. paleacea* LysM-RLKs in the perception
126 of COs and LCOs, we conducted binding assays using tagged receptors transiently expressed in
127 *Nicotiana benthamiana* cells. Firstly, the sub-cellular localization of the four receptor proteins tagged in
128 their C-terminus with mCherry was verified by confocal microscopy when co-expressed with the well-
129 known plasma-membrane resident Arabidopsis Flagellin Sensing 2 (FLS2) receptor which was fused
130 with GFP [25,26] (**Fig 4A**). For each receptor, the mCherry signal was visible on the epidermal cell
131 periphery and perfectly superimposed with the GFP signal, demonstrating the correct trafficking for all
132 four *M. paleacea* LysM-RLK fusion constructs to the plasma membrane in *N. benthamiana* (**Fig 4A**).
133 Next, microsomal preparations from leaf tissue expressing single LysM-RLK were mixed with increasing
134 concentrations of cross-linkable biotinylated chito-pentaose or chito-heptaose (hereafter CO5* and
135 CO7*, respectively) before detection of the biotin moieties and the mCherry tag by Western blot (**Fig**
136 **4B and D**). While none of the LYK receptors exhibited binding to CO5* or CO7* at concentrations up to
137 1 µM, a clear signal was observed for MpaLYR when challenged with only 100 nM of CO5* or CO7*.
138 (**Fig 4B and D**). The over-exposure of the streptavidin blots did not reveal any weak signals, thereby
139 suggesting that neither MpaLYKa, MpaLYKb nor MpaLYKc are able to bind CO5* or CO7* in these
140 conditions (**Fig S4**). To determine the affinity of the MpaLYR receptor with regards to COs, experiments
141 were conducted in which various concentrations of CO5* and CO7*, ranging from 1 nM to 2 µM, were
142 tested (**Fig 4C and E**). The presence of ligand-bound LYR proteins was observed at concentrations as
143 low as 10 nM of CO5* or 50 nM of CO7* (**Fig 4C and E**). Saturation of the signal between 250 and 500
144 nM indicate that the LYR receptor exhibits a high affinity for both short and long CO molecules. To
145 confirm these findings and test whether MpaLYR could also bind LCOs, a competition assay was
146 performed wherein MpaLYR-containing microsomes were simultaneously incubated with 100 nM CO5*
147 and 10-fold higher concentration (1 µM) of unlabelled chito-tetraose (CO4), CO7, or the major forms of
148 lipo-chitooligosaccharides produced by *R. irregularis*, LCO-V(C18:1, Fuc/MeFuc), hereafter
149 Fuc/MeFuc-LCO [27] (**Fig 4F**). Additionally, 1 µM of de-acetylated chitin (chitosan) fragments or 10
150 ng.µL^{-1} peptidoglycan fragments derived from *Bacillus subtilis* were used as negative controls. The
151 application of unlabelled CO4, CO7 or Fuc/MeFuc-LCOs resulted in a strong reduction in the binding of
152 CO5* to MpaLYR when compared to control condition in the absence of competitors. In contrast, the
153 application of bacterial peptidoglycan or chitosan fragments had no discernible effect on the binding of
154 CO5* to the MpaLYR receptor (**Fig 4F**). Collectively, these results support the conclusion that, within
155 the LysM-RLK family of *M. paleacea*, MpaLYR serves as the CO and LCO receptor.

COs and LCOs early signalling is impaired in *lyka* and *lyr* mutants of *Marchantia paleacea*

The function of MpaLYR, but not MpaLYKa, as a receptor for COs and LCOs was in apparent contradiction with the AM phenotypes of the corresponding mutants, with *MpaLYKa* but not *MpaLYR*, being critical for AM establishment. Therefore, we sought to correlate AM establishment and perception of AM fungus-derived signals by determining the signalling abilities of the different *M. palecea* receptor mutants in response to COs and LCOs. Ligand perception events by receptor-like kinases induce within seconds calcium influx into the cytosol in both immune and symbiotic contexts [28]. To use this physiological output, we generated a *M. paleacea* line expressing the cytosolic apoaequorin luminescent marker [29] under the control of the constitutive *MpoEF1α* promoter [30]. Once established and tested for suitable apoaequorin expression, this line served as a homogeneous background to re-create loss-of-function mutants using CRISPR/Cas9, as well as a control line expressing the Cas9 endonuclease alone (AEQ-cas9). Plants were then treated with CO7, CO4 or different LCOs, including Fuc/MeFuc-LCOs, LCO-IV(C18:1) (hereafter NS-LCOs) and LCO-IV(C18:1, S) (hereafter S-LCOs) [27,31].

To determine an effective working concentration for all molecules, we tested a range of concentrations starting at 10^{-6} M (1µM) followed by 10-fold series dilutions (**Fig 5A**). At the concentration of 1 µM, CO7, CO4 and Fuc/MeFuc-LCOs induced an increase in cytosolic calcium concentration in the *M. paleacea* control line that peaked at 5 minutes after application, before reaching back to the baseline at 15 minutes (**Fig 5A**). In contrast, NS-LCOs and S-LCOs failed to elicit a calcium response at this concentration (**Fig 5B**), suggesting variability in the potency of different LCO species. Importantly, water and dimethyl sulfoxide (DMSO) used to prepare stock solutions for CO4 and CO7 or LCOs, respectively, did not trigger any calcium variation in *M. paleacea* (**Fig S5**). Of the three active molecules, CO7 elicited the most pronounced response that gradually decreased in intensity and showed a slight delay when using diluted solutions. A clear response was still visible at 1 nM of CO7, although not statistically different from the lowest tested and poorly active concentration of 0.1 nM (**Fig 5A - insets**). In contrast, CO4 and Fuc/MeFuc-LCOs already failed to elicit a clear response at 0.1 µM, as evidenced by the shapes of the corresponding response curves (**Fig 5A**). In the following experiments, we have therefore chosen the highest concentration of 1 µM for all molecules. To verify whether cytosolic calcium variations occur at later time points, plant responses to CO7, CO4 and Fuc/MeFuc-LCOs were monitored over a one-hour time course. No additional calcium variation was apparent at later time points, suggesting that a 15 minutes time frame was sufficient to capture the entire cytosolic calcium response of *M. paleacea* to these molecules (**Fig 5C**). A five minutes pre-treatment with 1.5 mM lanthanum chloride (La^{3+}), a non-specific calcium channel blocker [32], completely abolished the cytosolic calcium variations triggered by CO7, CO4 or Fuc/MeFuc-LCOs (**Fig 5D**). This supports the

191 view that these cytosolic calcium variations are *bona fide* influxes of calcium originating from the
192 apoplast.

193 To determine whether this calcium influx triggered by CO7, CO4 and Fuc/MeFuc-LCOs seat
194 upstream or downstream of the CSSP, we analysed the response of two independent *symrk* mutants
195 generated in the aequorin-expressing *M. paleacea* background (**Fig S1 and Table S1**). The duration
196 and amplitude of the calcium influxes measured in AEQ-*symrk-1* and AEQ-*symrk-2* after 1 µM CO7,
197 CO4 or Fuc/MeFuc-LCOs treatments were similar to the control (**Fig 5E**). This result demonstrate that
198 this response is upstream SYMRK and distinct from calcium variations known as calcium spiking, which
199 are strictly dependent on CSSP activation. Taken together, our results show that CO7, CO4 and
200 Fuc/MeFuc-LCOs induce an early calcium influx in *M. paleacea* and that this physiological response
201 depends on a perception module that is independent of SYMRK.

202 Having established some characteristics of this CO7-, CO4- and Fuc/MeFuc-LCOs-induced
203 calcium influx in *M. paleacea*, we further investigated the function of each LysM-RLK in generating this
204 response. For that, we recovered two independent CRISPR/cas9-edited *M. paleacea* lines for each
205 receptor encoding gene in the aequorin-expressing background (**see. Table S1**). Next, we treated these
206 plants with 1 µM CO7, CO4 or Fuc/MeFuc-LCOs and monitored their calcium influx response in
207 comparison to the AEQ-cas9 control line (**Fig 6**). The duration and amplitude of the calcium influxes
208 obtained in AEQ-*lykb* and AEQ-*lykc* lines were comparable to the control for all three elicitors, whereas
209 AEQ-*lyka* and AEQ-*lyr* lines failed to respond to all treatments (**Fig 6**). Quantitative analysis of the area
210 under the curves and analysis of variance confirmed the similarity between control, AEQ-*lykb* and AEQ-
211 *lykc* and the differences between control and AEQ-*lyka* or AEQ-*lyr* in response to all elicitors (**Fig 6 –**
212 **bar graph insets**). To rule out the possibility that *lyka* and *lyr* mutations have a pleotropic effect on the
213 plants ability to mount a calcium response, we treated all genotypes with hydrogen peroxide (H_2O_2) at
214 a final concentration of 1 mM (**Fig S6**). All aequorin-expressing LysM-RLK mutants responded with an
215 immediate and robust calcium influx and quantitative analysis of the area under the curves and analysis
216 of variance confirmed that there was no difference between control, AEQ-*lyka* and AEQ-*lyr* mutants in
217 response to H_2O_2. In addition, the AM fungi colonisation status of AEQ-*lyka* and AEQ-*lyr*, the two non-
218 responsive mutants to COs and Fuc/MeFuc-LCOs, was evaluated after *R. irregularis* inoculation and
219 histological observations confirmed that AEQ-*lyka* was AM-defective (**Fig S7**). Conversely, as
220 previously described (**Figs 2 and 3, S2 and S3**), arbuscules were clearly visible in AEQ-cas9 and AEQ-
221 *lyr* plants with no differences in the size of the exclusion zone (**Fig S7**).
222 Collectively, these results demonstrate that MpaLYKa and MpaLYR are both required for the
223 perception of chitin-based molecules and their early signalling in *M. paleacea*.

CO7-induced transcriptomic changes are similarly affected in *lyka* and *lyr* mutants

The perception of non-self and the activation of corresponding signalling pathways in plants often culminate in adaptive transcriptomics reprogramming. Having established that early signalling in response to fungal molecules was blocked in both the *lyka* and *lyr* mutants, we then tested whether a later response such as gene induction was also affected in these mutants. First, we performed genome-wide transcriptomics of *M. paleacea* empty vector control plants after a one-hour treatment with 1 µM of CO7 or CO4. When compared to treatment with water only, CO7 and CO4 induced a statistically significant differential expression for 444 and 108 genes (p-adjusted value ≤ 0.05), respectively (**Table S2**). Of the differentially expressed genes (DEGs) identified in response to CO7, 195 were up-regulated with a log2 fold induction (log2FC) greater than 1, while 16 were down-regulated with a log2FC less than -1 (**Fig 7A**). In response to CO4, the application of identical log2FC cut-off values identified 45 genes that were up-regulated and two genes that were down-regulated (**Table S2**). Interestingly, 87% (94/108) of DEGs identified in response to CO4 are shared with CO7 (**Fig S8A**) and a direct comparison of the log2FC values in response to both treatments for the 108 CO4-responsive genes resulted in a Pearson's correlation coefficient of 0.91 (**Fig S8B**). The overlap and strong correlation between DEGs groups suggest that the transcriptomic response to CO4 represents a subset of the response to CO7 in *M. paleacea*. Furthermore, CO7 appears to be a more potent elicitor of gene reprogramming in this species, as evidenced by the fourfold higher number of identified DEGs in response to this molecule.

In order to gain insight into the most represented molecular functions, an InterPro domain enrichment analysis was performed on the up- and down-regulated genes in response to CO7 (**Fig S9 and Table S3**). A total of 18 InterPro terms were found to be significantly enriched among the subset of CO7-up-regulated genes. These included the terms "Leucine-rich repeat domain superfamily (IPR032675)," "Protein kinase domain" (IPR000719) and "WRKY domain superfamily" (IPR036576). The InterPro domain enrichment analysis using the set of 45 up-regulated genes after CO4 treatment yielded similar results, albeit with a lower number of significantly enriched terms (15 versus 18) (**Fig S10 and Table S3**). Taken together, these results suggest that CO perception in *M. paleacea* induces genes involved in cell-surface signalling and transcription. Conversely, the set of 16 down-regulated genes following CO7 treatment was significantly enriched in genes with functions related to photosynthesis and carbon fixation (**Fig S9B**), suggesting a potential growth inhibition trade-off after CO7 perception. The two down-regulated genes after CO4 treatment were not sufficient to perform a similar enrichment analysis.

In view of the overlap between the CO7 and CO4 transcriptomic responses observed in the control plants, we assessed the response of the *lyka* and *lyr* mutants to CO7 only. In the *lyka* mutant, CO7 treatment resulted in a statistically significant differential expression for 47 genes, with only two genes being up-regulated and two genes being down-regulated when the previously described log2FC

260 cut-off values were applied (**Fig 7A**). Moreover, none of these four up- or down-regulated genes were
261 present in the list of DEGs identified in the control plants (**Table S2**), suggesting that they may represent
262 noise rather than a true signal. In the *lyr* mutant, CO7 did not elicit any response in comparison to the
263 water treatment, as none of the two DEGs identified in this mutant showed a log2FC above the cut-off
264 values (**Fig 7A and Table S2**). A comparison across genotypes of the log2FC values from the DEGs
265 identified in the CO7-treated control plants further highlights the lack of response in the *lyka* and *lyr*
266 mutants (**Fig 7B**). Altogether, these results indicate that the *lyka* and *lyr* mutants of *M. paleacea* are
267 equally unable to induce gene expression in response to CO7.

Discussion

While single mutants in various *LYKs* in angiosperms have been observed to exhibit delayed or reduced colonization rates [10,33–37], none is completely defective for AM. In contrast, this work describes a single LYK mutant that displays an AM phenotype indistinguishable from those observed in mutants of the CSSP in angiosperms [4,5,38–43] or *M. paleacea* [8,9]. The absence of AM in *lyka* is consistent with the AM-defective phenotypes described in the *M. truncatula lyk8/lyk9* [14] and in the *L. japonicus lys6/lys7* double mutants [13]. This result obtained in a bryophyte species, combined with the phenotypes of the double mutants in legumes, corroborate the ancestral role of the LYK-I subclade in AM and substantiate the hypothesis that perception of fungal-derived molecule(s) by LysM-RLK is a prerequisite for AM establishment. Conversely, the loss of function of either *MpaLYKb* or *MpaLYKc* did not affect the establishment of AM. While no symbiotic function has yet been described for members of the LYK-III subclade (*MpaLYKc*), the co-orthologues of *MpaLYKb* (LYK-II subclade) in *L. japonicus*, *LjEPR3* and *LjEPR3a*, have been proposed to play regulatory functions during the accommodation of microbes [44,45]. *LYK-II* genes are also upregulated during AM in a range of plant species, including monocots [46], dicots, and bryophytes (for review, see Buendia et al., 2018). Interestingly, they are conserved in plants that form endosymbioses and are otherwise lost, a phylogenetic pattern that has been observed for genes of the CSSP [23]. These two lines of evidence support the existence of a conserved function for members of the LYK-II subclade in endosymbioses. The persistence of AM formation in the *LYK-II* mutants of *M. paleacea, L. japonicus* and rice suggests however that this function might come in complement to other signalling cues.

In addition to providing evidence supporting the involvement of MpaLYKa in AM, we demonstrate through measurement of cytosolic calcium influx that MpaLYKa is essential for both COs and LCOs perception. This calcium influx following CO and LCO perception in *M. paleacea* is independent of *SYMRK*, suggesting that it is distinct from the calcium spiking response observed in and around the nucleus, which strictly requires activation of the CSSP [47,48]. This observation is consistent with research in legumes, demonstrating the existence of an early calcium influx independent of the CSSP in response to Nod-factors [49] or CO8 and CO4 [50].

Perception of COs/LCOs in plants often involves heterocomplexes between LysM-RLKs of the LYK-I and LYR subclades [10], raising the possibility of an interaction between of MpaLYKa and MpaLYR for CO/LCO signalling in *M. paleacea*. In angiosperms, the LYR subgroup has expanded, giving rise, for example, to four and eleven paralogs in *Brachypodium distachyon* and *M. truncatula*, respectively [10]. The potential function of LYRs during AM has been extensively studied and single mutants have been tested for their symbiotic abilities in *M. truncatula* (*nfp* and *lyr4*) [51,52], *L. japonicus* (*Ljlys11*) [53], *Parasponia andersonii* (*Pannfp1*, *Pannfp2*) [37], tomato (*sllyk10*) [36], Petunia (*Phlyk10*) [36], barley (*rlk2* and *rlk10*) [39], *B. distachyon* (*bdlyr1* and *bdlyr2*) [54] and rice (*Osnfr5*) [55]. In addition, the double mutants *M. truncatula nfp/lyr4* [51] and *nfp/lyr1*, *L. japonicus lys11/nfr5* [53], *B. distachyon*

304 *bdlyr1/bdlyr2* [54] and barley *rlk2/rlk10* [39] were tested. Most of the single mutants displayed wild-type
305 level of colonisation by AM fungi, with the exception of tomato and petunia single mutants, and even
306 double mutants were either not or only partially affected in their AM fungi colonisation levels. One
307 hypothesis to explain these mixed results is the occurrence of significant variation in the number of
308 LysM-RLKs between these species and possible genetic redundancy or variable contributions from the
309 different paralogs in a species-specific manner. In *M. paleacea*, only one member of the *LYR* subgroup
310 is found and AM-phenotyping of the *lyr* loss-of-function mutants demonstrates the dispensable role of
311 this receptor for AM establishment in this species.

312 Interestingly, MpaLYR is able to bind short- and long-chain COs with high affinity. The ability of
313 MpaLYR to bind LCO molecules is probably due to the presence of the CO moiety of the LCO rather
314 than to a specific binding of the lipid moiety. The biochemical properties of MpaLYR are thus reminiscent
315 of those described for angiosperm LYR-IB receptors [10]. This supports an evolutionary scenario in
316 which receptors with specificity for LCO, such as members of the LYR-IA [12,36,56] and LYR-IIIA
317 [57,58] subclades, and receptors with specificity for long-chain versus short-chain COs, such as
318 members of the LYR-IIIC subclade [14,59], have emerged after the LYR expansion in angiosperms.
319 This could have led to a fine-tuning of the perception of symbionts and pathogens.

320 In contrast to MpaLYR, no binding activity towards chitin-based molecules could be detected in
321 any of the MpaLYK receptors. A similar observation has been reported in *M. truncatula* concerning the
322 ligand-binding abilities of LYR and LYK proteins [14]. However, both MpaLYR and MpaLYKa are
323 essential for the perception of chitinaceous compounds in *M. paleacea*. This suggests the existence of
324 MpaLYR/MpaLYK heterocomplexes for their perception, with a ligand-binding property conferred by
325 MpaLYR. Indeed, we have demonstrated that *lyr* and *lyka* mutants were incapable of producing a
326 calcium influx in response to CO7, CO4 or LCOs. Furthermore, CO7-dependent gene reprogramming
327 was entirely abolished in *lyr*, as it was in *lyka*. These results mirror the critical role of both MpoLYK1
328 and MpoLYR in CO7-triggered ROS production in the non-AM-host species *Marchantia polymorpha*
329 [20].

330 The identification of bacterial lipo-chitooligosaccharides (Nod-LCOs) that are essential for the
331 nitrogen-fixing symbiosis in legumes has led to the long-held hypothesis that functional analogues are
332 produced by AM fungi. The discoveries of AM fungi-produced LCOs and short-chain COs with symbiotic
333 activity in plants [52,60] provided compelling evidence to support this hypothesis. It has been proposed
334 that LCOs and short-chain COs represent a blend of symbiotic signals produced by AM fungi to initiate
335 symbiotic responses [52,60,61]. However, it remains unclear whether the perception of these molecules
336 by the host is a prerequisite for AM establishment. Interestingly, other compounds, such as CO8, can
337 induce similar molecular and cellular responses [14]. Furthermore, large-scale analyses of exudates
338 from sixty fungal species revealed that neither short-chain COs nor LCOs are specific to AM fungi
339 [27,62], raising questions about how plants can discriminate between beneficial and detrimental
340 organisms based on this class of compounds alone. Our work in *M. paleacea* suggests that AM

341 establishment can be uncoupled from COs and LCOs perception events and that MpaLYKa-dependent
342 perception of other type of symbiont-derived signal(s) occurs. The suite of *M. paleacea* mutants
343 developed here offer the opportunity to identify these elusive signal(s) in the future.

344 The study of mutants in bryophyte species which have lost the ability to form symbiosis allowed
345 discovering the ancestral function of LysM-RLK in plant immunity over the last decade [20,63]. Our work
346 extends this knowledge and proposes that LysM-RLK have been maintained in land plant genomes for
347 almost half a billion years not only to perceive pathogens but as readers of the biotic environment, both
348 for immunity and symbiosis.

349 Materials and methods

350 Phylogeny

351 To reconstruct the phylogeny of LysM-RLKs, a set of 102 protein sequences composed of 8
352 Marchantia genes and the set described by Buendia et al. (2018) supplemented with the *Lotus*
353 *japonicus* EPR3 and EPR3a sequences [45] was aligned using MUSCLE (v3.8). The phylogeny was
354 reconstructed using IQ-TREE v1.6.12 (http://iqtree.cibiv.univie.ac.at/) with the VT+F+I+G4 model and
355 support was provided with 1,000 ultra-fast bootstrap replicates [64–66]. The unrooted tree visualisation
356 was generated using iTOL [67] and adapted for presentation using InkScape.

357 Plant material, growth conditions and transformation

358 *Marchantia paleacea ssp. paleacea* wild-type plants were grown axenically *in vitro* from sterile
359 gemmae on ½ strength Gamborg B5 (G5768, Sigma) medium supplemented with 1.4 % agar (1330,
360 Euromedex) for 3 to 4 weeks in 16/8h photoperiod at 22°C/20°C. For transformation, ~20 plantlets were
361 blended 15 seconds in a sterile 250mL stainless steel bowl (Waring, USA) in 10mL of OM51C medium
362 [KNO_3 (2 g.L^{-1}), NH_4NO_3 (0.4 g.L^{-1}), $MgSO_4$ 7H_2O (0.37 g.L^{-1}), $CaCl_2$ 2H_2O (0.3 g.L^{-1}), KH_2PO_4 (0.275
363 g.L^{-1}), L-glutamine (0.3 g.L^{-1}), casamino-acids (1 g.L^{-1}), Na_2MoO_4 2H2O (0.25 mg.L^{-1}), $CuSO_4$ 5H_2O
364 (0.025 mg.L^{-1}), $CoCl_2$ 6H_2O (0.025 mg.L^{-1}), $ZnSO_4$ 7H2O (2 mg.L^{-1}), $MnSO_4$ H2O (10 mg.L^{-1}), H_3BO_3 (3
365 mg.L^{-1}), KI (0.75mg.L^{-1}), EDTA ferric sodium (36.7 mg.L^{-1}), myo-inositol (100 mg.L^{-1}), nicotinic acid (1
366 mg.L^{-1}), pyridoxine HCL (1 mg.L^{-1}), thiamine HCL (10mg.L^{-1})]. The blended plant tissues were
367 transferred to 250mL erlenmeyers containing 50 mL of OM51C and kept at 22°C/20°C, 16/8h
368 photoperiod, 200 RPM for 3 days. Co-cultures with *A. tumefaciens* (GV3101) containing constructs
369 were initiated by adding 1mL of saturated bacterial liquid culture (DO = 0,5, 50 mL final), acetosyringone
370 (100 µM final) and glutamine (0,5 g.L^{-1} final). After 3 days, plant fragments were washed by decantation
371 3 times with water and plated on ½ Gamborg containing 200 mg.L^{-1} amoxicillin (Levmentin, Laboratoires
372 Delbert, Fr.) and 10 mg.L^{-1} Hygromycin B (3250, Euromedex) or 50 nM Chlorsulfuron (34322-100MG
373 Sigma). Plant material is available in **Table S5**.

374 For AM experiments, *Marchantia paleacea ssp. paleacea* control and mutants were grown on
375 a zeolite substrate (50% fraction 1.0-2,5mm, 50% fraction 0,5-1.0-mm, Symbiom) in 7x7x8 cm pots with
376 a density of five thalli per pot. Pots were watered once a week with Long Ashton medium containing 7.5
377 µM of phosphate [68] and grown with a 16/8h photoperiod at 22°C/20°C for at least 2 weeks prior
378 inoculation with AM fungi. For calcium measurement, similar conditions were applied with the exception
379 of a higher plant density per pot and a growth duration of 4 weeks or plants were grown axenically *in*
380 *vitro* on 0,4% phytagel diluted in Long Ashton medium containing 7.5 µM of phosphate. For RNAseq
381 experiments, plants were grown axenically *in vitro* on 0,4% phytagel diluted in Long Ashton medium
382 containing 7.5 µM of phosphate for a duration of 4 weeks.

383 Cloning

384 The Golden Gate modular cloning system was used to prepare the plasmids as described in
385 *Schiessl et al* [69]. Level 1 and Level 2 empty vectors used in this study are listed in the **Table S5** and
386 held for distribution in the ENSA project core collection (https://www.ensa.ac.uk/). Other Level 0, Level
387 1 and Level 2 vectors containing constructs are listed in the **Table S5**. Coding sequences were either
388 domesticated in-house by PCR in the pUPD2 vector or synthesised and cloned into pMS (GeneArt,
389 Thermo Fisher Scientific, Waltham, USA).

390 Transient expression assays in *Nicotiana benthamiana*

391 *Agrobacterium tumefaciens* (GV3101) cultures carrying vectors of interest were grown under
392 agitation overnight at 28°C in liquid LB medium supplemented with adequate antibiotics. Cultures were
393 washed twice by centrifugation at 8000g and re-suspended in water supplemented with 50µM
394 acetosyringone. Bacteria concentrations were adjusted to OD_{600}=0.2 per construct prior infiltration of
395 the abaxial side of two months old *N. benthamiana* leaves using a 1 mL needle-less syringe.

396 Microscopy

397 For microscopy analyses, mCherry and GFP signals were sequentially acquired 48 hours after
398 *N. benthamiana* transfection using a Leica SP8 confocal microscope mounted with a FLUOTAR VISIR
399 25x/0.95NA water immersion objective (Leica). GFP was excited at 488 nm and detected from 500 to
400 535 nm; monomeric Cherry was excited at 552 nm and detected from 560 to 610 nm. Images were
401 processed using LasX (Leica).

402 Binding assays

403 Preparation of microsomal fraction was performed as previously described by Girardin et al.,
404 2019 [36]. CO5-biotin (CO5*) and CO7-biotin (CO7*) were synthesised as detailed by Cullimore et al.,
405 2023 [56] and Ding et al., 2024 [54] respectively. Binding assays were conducted using CO5* or CO7*

406 and competitors, mixed with the appropriate microsomal fraction in binding buffer (25 mM NaCacodylate
407 pH 6, 1 mM MgCl2, 1 mM CaCl2, 250 mM sucrose and protease inhibitors). Samples were incubated
408 for 30 min on ice and subsequently centrifuged for 30min at 31 000g and 4°C. Pellets were resuspended
409 in IP buffer (25 mM Tris-HCl pH7.5, 150 mM NaCl, 10% glycerol, supplemented with protease
410 inhibitors). Proteins were solubilized in IP buffer supplemented with 0.2% DDM for 1h at 4°C and
411 centrifuged during 30 min at 31 000g and 4°C. The supernatant was retrieved, and mCherry-tagged
412 receptors were immunoprecipitated using RFP-trap magnetic agarose beads (ChromoTek). Beads
413 were washed twice with IP buffer, and proteins were extracted in Laemmli buffer. Proteins were
414 separated by SDS-PAGE and transferred onto a nitrocellulose membrane using the Trans-Blot system
415 (Bio-rad) according to the manufacter's instructions. Membranes were blocked for 1h with 5% fat-free
416 milk in Tris-buffer Saline (TBS) supplemented with 0.1% Tween-20 (TBS-T). Membranes were
417 incubated for 1h with the appropriate antibodies: rabbit αRFP [70] (1:5000), αRabbit-Hrp (Millipore,
418 1:20000), and streptavidin-Hrp (Invitrogen, 1:3000). Hrp activity was detected using Clarity Western
419 ECL substrate (Bio-Rad) and observed with a ChemiDoc imager (Bio-Rad).

420 Generation of CRISPR mutants in *M. paleacea ssp. paleacea*

421 Constructs containing the *A. thaliana* codon-optimised SpCas9 [71] under the control of
422 *MpoEF1α* promoter and single guide RNAs (**Table S1**) under the *M. polymorpha* or *M. paleacea* U6
423 promoters were introduced in wild-type *M. paleacea.* Independent transformants for *lyka, lykb, lykc,* and
424 *lyr* were selected for AM phenotyping. A *M. paleacea* line expressing the calcium reporter aequorin
425 (AEQ) under the control of *MpoEF1α* promoter was re-transformed with the CRISPR/Cas9 vectors,
426 modified to contain a secondary selection marker (ChlorsulfuronR). Two independent mutant lines per
427 receptor were used for calcium influx assays.

428 Mycorrhization tests

429 Each pot containing 5 plants was inoculated with ~1,000 sterile spores of *Rhizophagus*
430 *irregularis* DAOM 197198 (Agronutrition). For the nursing experiment, thalli of empty-vector control and
431 *lyka* were transplanted in proximity to wild-type plants inoculated with *R. irregularis* spores more than
432 10 weeks before. Six- or ten-weeks post-inoculation (for nursing), thalli were cleared of chlorophyll using
433 ethanol 100% for 1 day before storage in an EDTA (0.5 mM). Cleared thalli were scanned with an
434 EPSON 11000XL and the distance between apical notches and the colonisation zone (naturally
435 coloured with a purple/brown pigment) were scored on using ImageJ. Large-scale mycorrhiza assays
436 were run independently twice.

437 For imaging, cleared thalli of control and mutants were embedded in 6% agarose and 100 µm thick
438 transversal and longitudinal sections were prepared using a Leica VT1000s vibratome. Sections were
439 incubated overnight in 10% K-OH (w/v) prior to three washes in PBS. Fungal membranes were stained
440 overnight using 1 $\mu g.mL^{-1}$ WGA-Alexa Fluor 488 (Sigma) diluted in PBS. Pictures were taken with a

441 Zeiss AxioZoom V16 binocular using a PlanApo Z 0.5X. objective and the ZEN software suite with
442 similar settings. Alexa Fluor was excited between 450 and 490 nm and emission collected between 500
443 and 550 nm.

444 Calcium influx measurements

445 Three to four weeks old plants were submerged in 2.5 µM coelenterazine-h (Interchim) diluted
446 in water for a minimum of 16 hours at room temperature and in the dark. Samples were then transferred
447 in a Berthold Sirius luminometer before treatments with a 250 µL aqueous solution of 1 µM CO7
448 dilutions, 1 µM CO4 (Elicityl, Crolles, France) or a 1 µM mixture of fucosyl/methylfucosyl LCO-V (C18:1,
449 Fuc/MeFuc), 1 µM non-sulphated LCOs and 1 µM sulphated LCOs. Luminescence was continuously
450 recorded for 15 min using a 1 sec interval. An equal volume of 2X lysis buffer [20% ETOH, 10mM
451 CaCl2, 2% NP-40] was injected to discharge the total luminescence left and light was collected for an
452 additional 5 min. Calcium concentrations were calibrated as previously done [72]. Graphs were
453 prepared using RStudio and the ggplot2 package by plotting signals from 10 to 900 seconds after
454 treatment, prior to assembly using the InkScape software. Areas under the curve from 10 to 900
455 seconds were calculated minus the baseline value, defined as the lowest value present in each trace.
456 A minimum of three traces for each experiment were recorded.

457 RNA extraction & RNA sequencing

458 Gemmae from control Cas9, *lyka-1* and *lyr-1* were surface sterilized with a nylon cell strainer
459 40µm (Falcon) in a bleach solution (~0.27%) for 1 minute and washed in water twice before plating on
460 ½ strength Gamborg B5 media and grown with a 16/8h photoperiod at 22°C/20°C. Plants were treated
461 or not with 1 µM elicitors for 1 hour before being frozen in liquid nitrogen. Tissues were ground with
462 mortar and pestle using liquid nitrogen prior total RNAs extraction using the RNA Plant and Fungi
463 NucleoSpin™ (Macherey-Nagel™). DNA was eliminated using the Macherey-Nagel™ Kit rDNase.
464 RNAs quality and quantity were determined by Nanodrop. Total RNAs were sent for sequencing to
465 Genewiz/Azenta (Leipzig, Germany). Illumina libraries were prepared with the NEBnext ultra II RNA
466 directional kit and sequenced on a NovaSeq platform. The samples were sequenced using a 2x150
467 Pair-End reads configuration.

468 RNAseq analysis

469 RNASeq raw reads from all described conditions were mapped against the genome of *M.*
470 *paleacea* [17] and counted using the Nextflow v23.10.0 [73] pipeline NF-CORE/RNASeq v3.14 [74] with
471 the options star_salmon to align and quantify reads, as well as '-nextseq 30 -length 50' as extra
472 parameters of TrimGalore v0.6.7 [75] to remove reads with quality lower than 30 or a length lower than
473 50bp. Ribosomal RNA were also removed through the option "-remove_ribo" using SortMeRNA v4.3.4

474 [76]. The pipeline was run under the GenoToul configuration (available here:
475 https://github.com/nfcore/configs/blob/master/docs/genotoul.md) and used the following softwares and
476 languages: bedtools v2.30.0 [77], R v4.0.3, v4.1.1 and v4.2.1 [78], DESEQ2 v1.28.0 [79]; dupradar
477 v1.28.0 [80], fastqc v 0.12.1 [81], fq v0.9.1 (https://github.com/stjude-rust-labs/fq), gffread v0.12.1 [82],
478 perl v5.26.2 [83], python v3.9.5 [84], rsem v1.3.1 [85], STAR v2.7.10a [86], picard v3.0.0 [87], qualimap
479 v2.3 [88], rseqc v5.02 [89], salmon v1.10.1 [90], summarizedExperiment v1.24.0 [91], samtools v1.16.1
480 [92], stringtie v2.2.1 [93], tximeta v1.12.0 [94], UCSC v377 and v445
481 (https://github.com/ucscGenomeBrowser/kent). The R package DESeq2 v1.42.1 was used with default
482 parameters for the differential gene expression analysis. Venn diagram was constructed using the
483 https://jvenn.toulouse.inrae.fr/ webserver with size modification in Inkscape. Enriched IPR terms were
484 determined using the R package clusterProfiler v4.12.3 [95], the DEGs with a log2FC threshold of |1|
485 as foreground and genes subjected DEG analysis (i.e. genes that were retained after removing the low
486 counts) as background. A template script is available at https://gist.github.com/LRSV-
487 MMbengue/beb55a608d6053c9aaa9257993c6bf6b

488 ## Statistical analyses

489 To evaluate differences versus control, student t-test or ANOVA followed by Tukey's HSD as
490 post-hoc test was performed using R.

491 # Figures

492 **Fig 1. *Marchantia paleacea* possesses four LysM Receptor-Like Kinases.**

493 Phylogenetic analysis of 102 LysM-RLKs from land plant species. Full-length protein sequences from
494 *A. thaliana* (AT), *S. lycopersicum* (Solyc), *O. sativa* (Os), *P. persica* (Prupe), *L. japonicus* (Lj), *M.*
495 *truncatula* (Medtr), *M. polymorpha* (Mapoly) and *M. paleacea* (Marpal) were aligned with MUSCLE prior
496 unrooted Maximum Likelihood phylogenetic tree construction using 1000 bootstraps resampling value.
497 Branch colours indicate bootstrap values. Four phylogenetic subclades are highlighted: LYK-I (blue),
498 LYK-II (orange), LYK-III (green), LYR (pink). *M. paleacea* proteins are labelled in red. The star sign
499 indicates the truncated LYKb homolog in *M. polymorpha*. Notable receptors for long-chain CO
500 perception in Arabidopsis or Nod factors perception in legumes are indicated with yellow or green dots,
501 respectively.

502 **Fig 2. *MpaLYKa* is essential for arbuscular mycorrhiza in *M. paleacea*.**

503 (**A - D**) Representative images of transversal sections of *M. paleacea* control (E.V.) or *lyk* mutants, as
504 indicated, six weeks after inoculation with *Rhizophagus irregularis*. Left panels are overlays of bright
505 fields (middle panels) and fluorescent (right panels) images. Wheat germ agglutinin (WGA) coupled to
506 Alexa Fluor 488 was used to detect fungal structures. Dashed line delimited insets are enlarged

507 underneath the original images. Scale bars are 500 µm and 200 µm for insets. (**E**) Quantitative analysis
508 of the exclusion zone length on mycorrhizal plants for control (E.V.) and two independent loss-of-
509 function mutants for each *LYK*. Fractions in bold grey represent mycorrhizal thalli over total thalli
510 assessed for each genotype. Different letters indicate differences to control inferred by ANOVA followed
511 by Tukey's HSD post-hoc test (p-value < 0.05). Control (E.V.) values are shared with Fig 3 and statistical
512 analysis was performed on the whole dataset. "nd" stands for not determined. (**F**) Longitudinal sections
513 of the *lyka-1* mutant 10 weeks after inoculation with *Rhizophagus irregularis*. (**G**) Longitudinal sections
514 of *M. paleacea* control (E.V.) or a *lyka-1* mutant six weeks after co-cultivation in close proximity with
515 wild-type mycorrhized *M. paleacea* nurse plants. Numbers of mycorrhized thalli over total thalli tested
516 are indicated. Scale bar = 200 µm.

517 **Fig 3. *MpaLYR* is dispensable for arbuscular mycorrhiza in *M. paleacea*.**

518 (**A**) Representative images of transversal sections of *M. paleacea* control (E.V.) or the *lyr-2* mutant six
519 weeks after inoculation with *Rhizophagus irregularis*. Left panels are overlays of bright field (middle
520 panels) and fluorescent (right panels) images. Wheat germ agglutinin (WGA) coupled to Alexa Fluor
521 488 was used to detect fungal structures. Dashed line delimited insets are enlarged underneath the
522 original images. Scale bars are 500 µm and 200 µm for insets. (**B**) Quantitative analysis of the
523 exclusion zone length on mycorrhizal plants for control (E.V.) and two *lyr* mutants. For each genotype,
524 fractions in bold grey represent mycorrhizal thalli over total thalli assessed. Different letters indicate
525 differences to control inferred by ANOVA followed by Tukey's HSD post-hoc test (p-value < 0.05).
526 Control values are shared with Fig 2 and statistical analysis was performed on the whole dataset.

527 **Fig 4. MpaLYR has high affinity for chito- and lipochito-oligosaccharides in *M. paleacea.***

528 (**A**) Confocal micrographs of *Nicotiana benthamiana* epidermal cells transiently co-expressing indicated
529 *M. paleacea* LysM-RLK-mCherry fusions (left panel) and the plasma membrane marker AtFLS2-GFP
530 (middle panel). Overlays including bright field images are shown (left panel). Scale bars = 25 µm. (**B-F**)
531 Microsomal fractions from *N. benthamiana* leaves expressing *M. paleacea* LysM-RLK-mCherry fusions,
532 as indicated, were utilised in binding assays with indicated concentrations of crosslinkable biotinylated
533 chitopentaose (CO5*) or chitoheptaose (CO7*). Ligand bound receptors and total immunopurified
534 receptors were detected using Streptavidin (top panels) or anti-RFP antibodies (bottom panels),
535 respectively. (**F**) CO5*-binding competition assays on MpaLYR using 10-fold higher concentrations of
536 CO4, CO7, Fuc/MeFuc-LCOs, PGN fragments or chitosan fragments relative to CO5*.

537 **Fig 5. Chito- and lipochito-oligosaccharides induce cytosolic calcium influx in *M. paleacea***
538 **independently of the common symbiosis pathway**.

539 Cytosolic calcium concentration variations in *M. paleacea* control plants (AEQ-cas9) in response to
540 decreasing concentrations of CO7, CO4 and Fuc/MeFuc-LCOs, as indicated, over a 15 minutes time

541 course. (**B**) Cytosolic calcium concentration variations in *M. paleacea* control plants (AEQ-cas9) in
542 response to 1 µM non-sulphated LCO (NS-LCO) or sulphated LCO (S-LCO), as indicated. (**C**) Cytosolic
543 calcium concentration variations in *M. paleacea* control plants (AEQ-cas9) in response to 1 µM CO7,
544 CO4 or Fuc/MeFuc-LCOs over a one-hour time course. (**D**) Effect of a 5 minutes pre-treatment with 1.5
545 mM lanthanum chloride on CO7-, CO4- or Fuc/MeFuc-LCO-induced calcium concentration variations.
546 (**E**) Cytosolic calcium concentration variations in two independent *M. paleacea symrk* mutant lines in
547 response to 1 µM CO7, CO4 or Fuc/MeFuc-LCOs. (**A-E**) Each trace represents the mean (line) ±
548 standard deviation (shading) from at least three replicates. (**A-D**) Bar graph insets represent the area
549 under the curves (A.U.C.) corrected for the baseline and different letters indicate significant differences
550 to control conditions inferred by ANOVA followed by Tukey's HSD post-hoc test (p-value < 0.05) for (A,
551 C) or Student t-test (p-value <0.01**; <0.001***) for (D).

552 **Fig 6. Chito- and lipochito-oligosaccharides-induced calcium influx response in *M. paleacea***
553 **depend on *MpaLYKa* and *MpaLYR*.**

554 Cytosolic calcium concentration variations in *M. paleacea* control (AEQ-cas9) or two independent
555 mutant lines for each *LysM-RLK* of *M. paleacea*, as indicated. Plants were treated with 1 µM CO7 (left),
556 1 µM CO4 (middle) or 1 µM Fuc/MeFuc-LCOs (right). Each trace represents the mean (line) ± standard
557 deviation (shading) from at least three replicates over a time course of 15 min. Bar graph insets
558 represent the area under the curves (A.U.C.) corrected for the baseline and different letters indicate
559 significant differences versus control inferred by ANOVA and Tukey's HSD post-hoc test (p-value <
560 0.05).

561 **Fig 7. *MpaLYKa* and *MpaLYR* are essential for gene induction in response to CO7.**

562 Number of significantly upregulated or downregulated genes (yellow or blue, respectively) in CO7-
563 treated plants for one-hour (control, *lyka* and *lyr*) relative to non-treated plants. DEGs are statistically
564 significant (p-value adjusted < 0.05 and |log2FC| ≥ 1). (**B**) Heatmap of the expression pattern in *lyka*
565 and *lyr* mutants compared with the control in plants treated with 1µM CO7. Displayed fold changes are
566 statistically significant for the control (p-value adjusted < 0.05).

567 Supporting information

568 **Fig S1. Protospacers positions for generating loss-of-function RLK mutants in *M. paleacea*.**
569 Gene structure representation of the four *M. paleacea LysM-RLKs* and *SYMRK:* exons (grey boxes),
570 introns (black line), signal peptides and transmembrane domain coding sequences are highlighted in
571 brown and green, respectively. Arrowheads point at protospacers positions used for generating
572 CRISPR/Cas9 loss-of-function mutants. For *SYMRK*, a polycistronic RNA construct was designed to
573 generate two guide RNAs.
574

575 **Fig S2. Longitudinal sections of *M. paleacea lyk* mutants and exclusion zone measurements.**
576 (**A**) Representative images of longitudinal sections of *M. paleacea* control (E.V.) or *lyk* mutants, as
577 indicated, six weeks after inoculation with *R. irregularis*. Left panels are overlays of bright field (middle
578 panels) and fluorescent (right panels) images. Wheat germ agglutinin (WGA) coupled to Alexa Fluor
579 488 was used to detect fungal structures. Dashed line delimited insets are enlarged underneath the
580 original images. Scale bars are 500 µm and 200 µm for insets. (**B**) Quantitative analysis of the
581 exclusion zone length on mycorrhizal plants for control (E.V.) and loss-of-function *lyk* mutants. For each
582 genotype, fractions in bold grey represent mycorrhizal thalli over total thalli assessed. Different letters
583 indicate differences to control inferred by ANOVA followed by Tukey's HSD post-hoc test (p-value <
584 0.05). Control (E.V.) values are shared with **Fig S3** and statistical analysis was performed on the whole
585 dataset. "nd" stands for not determined.
586
587 **Fig S3. Longitudinal sections of *M. paleacea lyr* mutant and exclusions zones measurements.**
588 (**A**) Representative images of longitudinal sections of *M. paleacea* control (E.V.) or the *lyr-2* mutants six
589 weeks after inoculation with *R. irregularis*. Left panels are overlays of bright field (middle panels) and
590 fluorescent (right panels) images. Wheat germ agglutinin (WGA) coupled to Alexa Fluor 488 was used
591 to detect fungal structures. Dashed line delimited insets are enlarged underneath the original images.
592 Scale bars are 500 µm and 200 µm for insets. (**B**) Quantitative analysis of the exclusion zone length on
593 mycorrhizal plants for control (E.V.) and two independent *lyr* mutants. For each genotype, fractions in
594 bold grey represent mycorrhizal thalli over total thalli assessed. Different letters indicate differences to
595 control inferred by ANOVA followed by Tukey's HSD post-hoc test (p-value < 0.05). Control (E.V.)
596 values are shared with **Fig S2** and statistical analysis was performed on the whole dataset.
597
598 **Fig S4. MpaLYR has high affinity for chito- and lipochito-oligosaccharides in *M. paleacea.***
599 (**A**) and (**B**) are identical to the panels shown in **Fig 4B** and **Fig 4D**, respectively, but with over-
600 exposition of the streptavidin-HRP detection. RFP detection was not modified.
601
602 **Fig S5. DMSO and water alone do not elicit calcium influx in *M. paleacea.***
603 Cytosolic calcium concentration variations in *M. paleacea* control plants (AEQ-cas9) in response to (**A**)
604 0.1% dimethyl sulfoxide (DMSO) diluted in water or (**B**) water alone, over a time course of 15 min. (**A-**
605 **B**) Each trace represents the mean (line) ± standard deviation (shading) from at least three replicates.
606
607 **Fig S6. *M. paleacea* LysM-RLK mutants produce a calcium influx in response to hydrogen**
608 **peroxide.**
609 Cytosolic calcium concentration variations in *M. paleacea* control (AEQ-cas9) or two independent
610 mutant lines for each *LysM-RLK*, as indicated, and treated with 1mM hydrogen peroxide diluted in water.
611 Each trace represents the mean (line) ± standard deviation (shading) from three replicates over a time
612 course of 15 min. Bar graph insets represent the area under the curves (A.U.C.) corrected for the

613 baseline and different letters indicate significant differences versus control inferred by ANOVA and
614 Tukey's HSD post-hoc test (p-value < 0.05).
615 **Fig S7. *lyka* and *lyr* mycorrhizal phenotypes in the *M. paleacea* aequorin-expressing**
616 **background.**
617 (**A-C**) Representative images of transversal sections of *M. paleacea* control (AEQ/cas9), one AEQ/*lyka*
618 and one AEQ/*lyr* mutant, six weeks after inoculation with *Rhizophagus irregularis*. Left panels are
619 overlays of bright field (middle panels) and fluorescent (right panels) images. Wheat germ agglutinin
620 (WGA) coupled to Alexa Fluor 488 was used to detect fungal structures. Dashed line delimited insets
621 are enlarged underneath the original images. Scale bars are 500 µm and 200 µm for insets. (**D**)
622 Quantitative analysis of the exclusion zone length on mycorrhizal plants for control (AEQ/cas9) and two
623 independent *lyka* and *lyr* mutants. For each genotype, fractions in bold grey represent mycorrhizal thalli
624 over total thalli assessed.
625
626 **Fig S8. Transcriptomics response to CO4 is a subset of the CO7 response.**
627 (**A**) Venn diagram of differentially expressed genes (DEGs) in control plants after one-hour CO7 or CO4
628 treatment versus water (p adjusted value < 0.05). (**B**) Scatter plot of the log2 fold changes from the 108
629 DEGs in response to CO4 (x-axis) against their corresponding log2 fold changes in response to CO7
630 (y-axis). The 45 up-regulated and 2 down-regulated genes in response to CO4 (|log2FC| ≥ 1 – dashed
631 grey bars) are highlighted in red and blue, respectively. The Pearson's correlation coefficient between
632 CO7 and CO4 log2FC values is indicated.
633
634 **Fig S9. InterPro terms enrichment analyses in response to CO7.**
635 InterPro terms enrichment among up-regulated (**A**) and down-regulated (**B**) genes after 1µM CO7
636 treatment. DEGs are statistically significant (p-value adjusted < 0.05 and |log2FC| ≥ 1).
637
638 **Fig S10. InterPro terms enrichment analysis in response to CO4.**
639 InterPro terms enrichment among up-regulated genes after 1µM CO4 treatment. DEGs are statistically
640 significant (p-value adjusted < 0.05 and |log2FC| ≥ 1).

641 **S1 Table. List of protospacers sequences used for gene editions.**
642 **S2 Table. List of differentially regulated genes in response to CO7 and CO4 in *M. paleacea* WT**
643 **and CO7 for *lyka* and *lyr*.**
644 **S3 Table. InterPro terms enrichment analyses in response to CO7 and CO4.**
645 **S4 Table. List of primers for genotyping edited lines.**
646 **S5 Table. List of constructs and selected lines used in this study.**

Acknowledgements

We would like to thank Vincent Garrigues, Manon Grousset, Lou Battaglia and Madeleine Baker for their technical assistance and Didier Aldon for critically reading the manuscript. E.T. is supported by a PhD grant from the French Ministry of Higher Education and Research. Research performed at LRSV was supported by the 'Laboratoires d'Excellence (LABEX)' TULIP (ANR-10-LABX-41) and the 'École Universitaire de Recherche (EUR)' TULIP-GS (ANR-18-EURE-0019). P-M.D. is supported by the project Engineering Nitrogen Symbiosis for Africa (ENSA) funded through a grant to the University of Cambridge by the Bill and Melinda Gates Foundation (OPP1172165) and the UK Foreign, Commonwealth and Development Office as Engineering Nitrogen Symbiosis for Africa (OPP1172165) and by funding from the European Research Council (ERC) under the European Union's Horizon 2020 research and innovation programme (grant agreement no. 101001675 - ORIGINS) to P-M.D. We are grateful to the genotoul bioinformatics platform Toulouse Occitanie (https://bioinfo.genotoul.fr/) for providing computing resources. S.F. acknowledges NanoBio ICMG (UAR 2607) for providing access to mass spectrometry and NMR facilities and the French National Research Agency-ANR through LABEX ARCANE/EUR CBH-EUR-GS (ANR-17-EURE-0003), Glyc@Alps (ANR-15-IDEX-02), and Carnot Polynat (CARN-025-01) for partial financial support.

Author contributions

E.T. and M.M. designed and coordinated the experiments. S.F. provided material. E.T., S.G., M.R., M.O., D.L., J.K. and M.M. conducted experiments. E.T., D.L, B.L., P.M.D. and M.M. wrote the manuscript. M.M. coordinated the project.

References

1. Smith SE, Read DJ. Mycorrhizal symbiosis. Elsevier; 2002. doi:10.1016/B978-0-12-652840-4.X5000-1

2. Kodama K, Rich MK, Yoda A, Shimazaki S, Xie X, Akiyama K, et al. An ancestral function of strigolactones as symbiotic rhizosphere signals. Nat Commun. 2022;13: 3974. doi:10.1038/s41467-022-31708-3

3. Kistner C, Parniske M. Evolution of signal transduction in intracellular symbiosis. Trends in Plant Science. 2002;7: 511–518. doi:10.1016/S1360-1385(02)02356-7

4. Stracke S, Kistner C, Yoshida S, Mulder L, Sato S, Kaneko T, et al. A plant receptor-like kinase required for both bacterial and fungal symbiosis. Nature. 2002;417: 959–962. doi:10.1038/nature00841

5. Endre G, Kereszt A, Kevei Z, Mihacea S, Kaló P, Kiss GB. A receptor kinase gene regulating symbiotic nodule development. Nature. 2002;417: 962–966. doi:10.1038/nature00842

6. Miyata K, Hosotani M, Akamatsu A, Takeda N, Jiang W, Sugiyama T, et al. OsSYMRK plays an essential role in AM symbiosis in Rice (*Oryza sativa*). Plant and Cell Physiology. 2023;64: 378–391. doi:10.1093/pcp/pcad006

7. Jin Y, Chen Z, Yang J, Mysore KS, Wen J, Huang J, et al. IPD3 and IPD3L function redundantly in rhizobial and mycorrhizal symbioses. Front Plant Sci. 2018;9: 267. doi:10.3389/fpls.2018.00267

682 8. Vernié T, Rich M, Pellen T, Teyssier E, Garrigues V, Chauderon L, et al. Conservation of symbiotic signalling
683 across 450 million years of plant evolution. bioRxiv; 2024. p. 2024.01.16.575147.
684 doi:10.1101/2024.01.16.575147

685 9. Lam AHC, Cooke A, Wright H, Lawson DM, Charpentier M. Evolution of endosymbiosis-mediated nuclear
686 calcium signaling in land plants. Current Biology. 2024;39: 1–9. doi:10.1016/j.cub.2024.03.063

687 10. Buendia L, Girardin A, Wang T, Cottret L, Lefebvre B. LysM Receptor-Like Kinase and LysM Receptor-Like
688 Protein families: An update on phylogeny and functional characterization. Front Plant Sci. 2018;9: 1531.
689 doi:10.3389/fpls.2018.01531

690 11. Madsen EB, Madsen LH, Radutoiu S, Olbryt M, Rakwalska M, Szczyglowski K, et al. A receptor kinase gene
691 of the LysM type is involved in legume perception of rhizobial signals. Nature. 2003;425: 637–640.
692 doi:10.1038/nature02045

693 12. Broghammer A, Krusell L, Blaise M, Sauer J, Sullivan JT, Maolanon N, et al. Legume receptors perceive the
694 rhizobial lipochitin oligosaccharide signal molecules by direct binding. Proc Natl Acad Sci USA. 2012;109:
695 13859–13864. doi:10.1073/pnas.1205171109

696 13. Fukuda H, Mamiya R, Akamatsu A, Takeda N. Two LysM receptor-like kinases regulate arbuscular
697 mycorrhiza through distinct signaling pathways in *Lotus japonicus*. New Phytologist. 2024; nph.19863.
698 doi:10.1111/nph.19863

699 14. Zhang J, Sun J, Chiu CH, Landry D, Li K, Wen J, et al. A receptor required for chitin perception facilitates
700 arbuscular mycorrhizal associations and distinguishes root symbiosis from immunity. Current Biology. 2024;
701 1–13. doi:10.1016/j.cub.2024.03.015

702 15. Puttick MN, Morris JL, Williams TA, Cox CJ, Edwards D, Kenrick P, et al. The interrelationships of land plants
703 and the nature of the ancestral embryophyte. Current Biology. 2018;28: 733–745.
704 doi:10.1016/j.cub.2018.01.063

705 16. Delaux P-M, Hetherington AJ, Coudert Y, Delwiche C, Dunand C, Gould S, et al. Reconstructing trait
706 evolution in plant evo–devo studies. Current Biology. 2019;29: R1110–R1118.
707 doi:10.1016/j.cub.2019.09.044

708 17. Rich MK, Vigneron N, Libourel C, Keller J, Xue L, Hajheidari M, et al. Lipid exchanges drove the evolution
709 of mutualism during plant terrestrialization. Science. 2021;372: 864–868. doi:10.1126/science.abg0929

710 18. Delaux P-M, Radhakrishnan GV, Jayaraman D, Cheema J, Malbreil M, Volkening JD, et al. Algal ancestor
711 of land plants was preadapted for symbiosis. Proc Natl Acad Sci USA. 2015;112: 13390–13395.
712 doi:10.1073/pnas.1515426112

713 19. Nishiyama T, Sakayama H, De Vries J, Buschmann H, Saint-Marcoux D, Ullrich KK, et al. The Chara
714 genome: Secondary complexity and implications for plant terrestrialization. Cell. 2018;174: 448–464.
715 doi:10.1016/j.cell.2018.06.033

716 20. Yotsui I, Matsui H, Miyauchi S, Iwakawa H, Melkonian K, Schlüter T, et al. LysM-mediated signaling in
717 *Marchantia polymorpha* highlights the conservation of pattern-triggered immunity in land plants. Current
718 Biology. 2023;33: 3732–3746. doi:10.1016/j.cub.2023.07.068

719 21. Miya A, Albert P, Shinya T, Desaki Y, Ichimura K, Shirasu K, et al. CERK1, a LysM receptor kinase, is
720 essential for chitin elicitor signaling in *Arabidopsis*. Proc Natl Acad Sci USA. 2007;104: 19613–19618.
721 doi:10.1073/pnas.0705147104

722 22. Radutoiu S, Madsen LH, Madsen EB, Felle HH, Umehara Y, Grønlund M, et al. Plant recognition of symbiotic
723 bacteria requires two LysM receptor-like kinases. Nature. 2003;425: 585–592. doi:10.1038/nature02039

724 23. Radhakrishnan GV, Keller J, Rich MK, Vernié T, Mbadinga Mbadinga DL, Vigneron N, et al. An ancestral
725 signalling pathway is conserved in intracellular symbioses-forming plant lineages. Nat Plants. 2020;6: 280–
726 289. doi:10.1038/s41477-020-0613-7

727 24. Humphreys CP, Franks PJ, Rees M, Bidartondo MI, Leake JR, Beerling DJ. Mutualistic mycorrhiza-like
728 symbiosis in the most ancient group of land plants. Nat Commun. 2010;1: 103. doi:10.1038/ncomms1105

729 25. Robatzek S, Chinchilla D, Boller T. Ligand-induced endocytosis of the pattern recognition receptor FLS2 in
730 *Arabidopsis*. Genes Dev. 2006;20: 537–542. doi:10.1101/gad.366506

731 26. Beck M, Zhou J, Faulkner C, MacLean D, Robatzek S. Spatio-temporal cellular dynamics of the *Arabidopsis*
732 flagellin receptor reveal activation status-dependent endosomal sorting. The Plant Cell. 2012;24: 4205–
733 4219. doi:10.1105/tpc.112.100263

734 27. Rush TA, Puech-Pagès V, Bascaules A, Jargeat P, Maillet F, Haouy A, et al. Lipo-chitooligosaccharides as
735 regulatory signals of fungal growth and development. Nat Commun. 2020;11: 3897. doi:10.1038/s41467-
736 020-17615-5

737 28. Zipfel C, Oldroyd GED. Plant signalling in symbiosis and immunity. Nature. 2017;543: 328–336.
738 doi:10.1038/nature22009

739 29. Knight MR, Read ND, Campbell AK, Trewavas AJ. Imaging calcium dynamics in living plants using semi-
740 synthetic recombinant aequorins. The Journal of Cell Biology. 1993;121.

741 30. Althoff F, Kopischke S, Zobell O, Ide K, Ishizaki K, Kohchi T, et al. Comparison of the MpEF1α and CaMV35
742 promoters for application in *Marchantia polymorpha* overexpression studies. Transgenic Res. 2014;23: 235–
743 244. doi:10.1007/s11248-013-9746-z

744 31. Maillet F, Fournier J, Mendis HC, Tadege M, Wen J, Ratet P, et al. *Sinorhizobium meliloti* succinylated high-
745 molecular-weight succinoglycan and the *Medicago truncatula* LysM receptor-like kinase MtLYK10 participate
746 independently in symbiotic infection. The Plant Journal. 2020;102: 311–326. doi:10.1111/tpj.14625

747 32. Lewis BD, Spalding EP. Nonselective block by La 3+ of *Arabidopsis* ion channels Involved in signal
748 transduction. Journal of Membrane Biology. 1998;162: 81–90. doi:10.1007/s002329900344

749 33. Miyata K, Hasegawa S, Nakajima E, Nishizawa Y, Kamiya K, Yokogawa H, et al. OsCERK2/OsRLK10, a
750 homolog of OsCERK1, has a potential role for chitin-triggered immunity and arbuscular mycorrhizal
751 symbiosis in rice. Plant Biotechnology. 2022;39: 119–128. doi:10.5511/plantbiotechnology.21.1222a

752 34. Miyata K, Kozaki T, Kouzai Y, Ozawa K, Ishii K, Asamizu E, et al. The bifunctional plant receptor, OsCERK1,
753 regulates both chitin-triggered immunity and arbuscular mycorrhizal symbiosis in Rice. Plant and Cell
754 Physiology. 2014;55: 1864–1872. doi:10.1093/pcp/pcu129

755 35. Gibelin-Viala C, Amblard E, Puech-Pages V, Bonhomme M, Garcia M, Bascaules-Bedin A, et al. The
756 *Medicago truncatula* LysM receptor-like kinase LYK9 plays a dual role in immunity and the arbuscular
757 mycorrhizal symbiosis. New Phytologist. 2019;223: 1516–1529. doi:10.1111/nph.15891

758 36. Girardin A, Wang T, Ding Y, Keller J, Buendia L, Gaston M, et al. LCO receptors involved in arbuscular
759 mycorrhiza are functional for rhizobia perception in legumes. Current Biology. 2019;29: 4249-4259.e5.
760 doi:10.1016/j.cub.2019.11.038

761 37. Rutten L, Miyata K, Roswanjaya YP, Huisman R, Bu F, Hartog M, et al. Duplication of symbiotic lysin motif
762 receptors predates the evolution of nitrogen-fixing nodule symbiosis. Plant Physiol. 2020;184: 1004–1023.
763 doi:10.1104/pp.19.01420

764 38. Gutjahr C, Banba M, Croset V, An K, Miyao A, An G, et al. Arbuscular mycorrhiza–specific signaling in rice
765 transcends the common symbiosis signaling pathway. The Plant Cell. 2008;20: 2989–3005.
766 doi:10.1105/tpc.108.062414

767 39. Li X-R, Sun J, Albinsky D, Zarrabian D, Hull R, Lee T, et al. Nutrient regulation of lipochitooligosaccharide
768 recognition in plants via NSP1 and NSP2. Nat Commun. 2022;13: 6421. doi:10.1038/s41467-022-33908-3

769 40. Yano K, Yoshida S, Müller J, Singh S, Banba M, Vickers K, et al. CYCLOPS, a mediator of symbiotic
770 intracellular accommodation. Proc Natl Acad Sci USA. 2008;105: 20540–20545.
771 doi:10.1073/pnas.0806858105

41. Messinese E, Mun J-H, Yeun LH, Jayaraman D, Rougé P, Barre A, et al. A novel nuclear protein interacts with the symbiotic DMI3 calcium- and calmodulin-dependent protein kinase of *Medicago truncatula*. MPMI. 2007;20: 912–921. doi:10.1094/MPMI-20-8-0912

42. Lévy J, Bres C, Geurts R, Chalhoub B, Kulikova O, Duc G, et al. A putative Ca^{2+} and calmodulin-dependent protein kinase required for bacterial and fungal symbioses. Science. 2004;303: 1361–1364. doi:10.1126/science.1093038

43. Catoira R, Galera C, de Billy F, Penmetsa RV, Journet E-P, Maillet F, et al. Four genes of *Medicago truncatula* controlling components of a nod factor ttransduction pathway. The Plant Cell. 2000;12: 1647–1665.

44. Kawaharada Y, Kelly S, Nielsen MW, Hjuler CT, Gysel K, Muszyński A, et al. Receptor-mediated exopolysaccharide perception controls bacterial infection. Nature. 2015;523: 308–312. doi:10.1038/nature14611

45. Kelly S, Hansen SB, Rübsam H, Saake P, Pedersen EB, Gysel K, et al. A glycan receptor kinase facilitates intracellular accommodation of arbuscular mycorrhiza and symbiotic rhizobia in the legume *Lotus japonicus*. Haney CH, editor. PLoS Biol. 2023;21: e3002127. doi:10.1371/journal.pbio.3002127

46. Roth R, Chiapello M, Montero H, Gehrig P, Grossmann J, O'Holleran K, et al. A rice Serine/Threonine receptor-like kinase regulates arbuscular mycorrhizal symbiosis at the peri-arbuscular membrane. Nat Commun. 2018;9: 4677. doi:10.1038/s41467-018-06865-z

47. Wais RJ, Galera C, Oldroyd G, Catoira R, Penmetsa RV, Cook D, et al. Genetic analysis of calcium spiking responses in nodulation mutants of *Medicago truncatula*. Proc Natl Acad Sci USA. 2000;97: 13407–13412. doi:10.1073/pnas.230439797

48. Kelner A, Leitão N, Chabaud M, Charpentier M, de Carvalho-Niebel F. Dual color sensors for simultaneous analysis of calcium signal dynamics in the nuclear and cytoplasmic compartments of plant cells. Front Plant Sci. 2018;9: 245. doi:10.3389/fpls.2018.00245

49. Shaw SL, Long SR. Nod Factor elicits two separable calcium responses in *Medicago truncatula* root hair cells. Plant Physiology. 2003;131: 976–984. doi:10.1104/pp.005546

50. Binci F, Offer E, Crosino A, Sciascia I, Kleine-Vehn J, Genre A, et al. Spatially and temporally distinct Ca2+ changes in *Lotus japonicus* roots orient fungal-triggered signalling pathways towards symbiosis or immunity. Gifford M, editor. Journal of Experimental Botany. 2024;75: 605–619. doi:10.1093/jxb/erad360

51. Feng F, Sun J, Radhakrishnan GV, Lee T, Bozsóki Z, Fort S, et al. A combination of chitooligosaccharide and lipochitooligosaccharide recognition promotes arbuscular mycorrhizal associations in *Medicago truncatula*. Nat Commun. 2019;10: 5047. doi:10.1038/s41467-019-12999-5

52. Maillet F, Poinsot V, André O, Puech-Pagès V, Haouy A, Gueunier M, et al. Fungal lipochitooligosaccharide symbiotic signals in arbuscular mycorrhiza. Nature. 2011;469: 58–63. doi:10.1038/nature09622

53. Rasmussen SR, Füchtbauer W, Novero M, Volpe V, Malkov N, Genre A, et al. Intraradical colonization by arbuscular mycorrhizal fungi triggers induction of a lipochitooligosaccharide receptor. Sci Rep. 2016;6: 29733. doi:10.1038/srep29733

54. Ding Y, Gasciolli V, Medioni L, Gaston M, de-Regibus A, Rem-blière C, et al. A new group of LysM-RLKs involved in symbiotic signal perception and arbuscular mycorrhiza establishment. biorxiv. 2024 [cited 19 Mar 2024]. doi:10.1101/2024.03.06.583654

55. Miyata K, Hayafune M, Kobae Y, Kaku H, Nishizawa Y, Masuda Y, et al. Evaluation of the role of the LysM Receptor-Like Kinase, OsNFR5/OsRLK2 for AM symbiosis in Rice. Plant Cell Physiol. 2016;57: 2283–2290. doi:10.1093/pcp/pcw144

56. Cullimore J, Fliegmann J, Gasciolli V, Gibelin-Viala C, Carles N, Luu T-B, et al. Evolution of lipochitooligosaccharide binding to a LysM-RLK for nodulation in *Medicago truncatula*. Plant and Cell Physiology. 2023;64: 746–757. doi:10.1093/pcp/pcad033

818 57. Malkov N, Fliegmann J, Rosenberg C, Gasciolli V, Timmers ACJ, Nurisso A, et al. Molecular basis of lipo-
819 chitooligosaccharide recognition by the lysin motif receptor-like kinase LYR3 in legumes. Biochemical
820 Journal. 2016;473: 1369–1378. doi:10.1042/BCJ20160073

821 58. Wang T, Gasciolli V, Gaston M, Medioni L, Cumener M, Buendia L, et al. LysM receptor-like kinases involved
822 in immunity perceive lipo-chitooligosaccharides in mycotrophic plants. Plant Physiology. 2023; kiad059.
823 doi:10.1093/plphys/kiad059

824 59. Cao Y, Liang Y, Tanaka K, Nguyen CT, Jedrzejczak RP, Joachimiak A, et al. The kinase LYK5 is a major
825 chitin receptor in *Arabidopsis* and forms a chitin-induced complex with related kinase CERK1. eLife. 2014;3:
826 e03766. doi:10.7554/eLife.03766

827 60. Genre A, Chabaud M, Balzergue C, Puech-Pagès V, Novero M, Rey T, et al. Short-chain chitin oligomers
828 from arbuscular mycorrhizal fungi trigger nuclear Ca^{2+} spiking in *Medicago truncatula* roots and their
829 production is enhanced by strigolactone. New Phytologist. 2013;198: 190–202. doi:10.1111/nph.12146

830 61. Genre A, Lanfranco L, Perotto S, Bonfante P. Unique and common traits in mycorrhizal symbioses. Nat Rev
831 Microbiol. 2020;18: 649–660. doi:10.1038/s41579-020-0402-3

832 62. Cope KR, Bascaules A, Irving TB, Venkateshwaran M, Maeda J, Garcia K, et al. The ectomycorrhizal fungus
833 *Laccaria bicolor* produces lipochitooligosaccharides and uses the common symbiosis pathway to colonize
834 *Populus* roots. Plant Cell. 2019;31: 2386–2410. doi:10.1105/tpc.18.00676

835 63. Bressendorff S, Azevedo R, Kenchappa CS, Ponce De León I, Olsen JV, Rasmussen MW, et al. An innate
836 immunity pathway in the moss *Physcomitrella patens*. The Plant Cell. 2016;28: 1328–1342.
837 doi:10.1105/tpc.15.00774

838 64. Kalyaanamoorthy S, Minh BQ, Wong TKF, von Haeseler A, Jermiin LS. ModelFinder: fast model selection
839 for accurate phylogenetic estimates. Nat Methods. 2017;14: 587–589. doi:10.1038/nmeth.4285

840 65. Nguyen L-T, Schmidt HA, Von Haeseler A, Minh BQ. IQ-TREE: A fast and effective stochastic algorithm for
841 estimating maximum-likelihood phylogenies. Molecular Biology and Evolution. 2015;32: 268–274.
842 doi:10.1093/molbev/msu300

843 66. Hoang DT, Chernomor O, Von Haeseler A, Minh BQ, Vinh LS. UFBoot2: Improving the ultrafast bootstrap
844 approximation. Molecular Biology and Evolution. 2018;35: 518–522. doi:10.1093/molbev/msx281

845 67. Letunic I, Bork P. Interactive Tree Of Life (iTOL) v5: an online tool for phylogenetic tree display and
846 annotation. Nucleic Acids Research. 2021;49: W293–W296. doi:10.1093/nar/gkab301

847 68. Balzergue C, Puech-Pagès V, Bécard G, Rochange SF. The regulation of arbuscular mycorrhizal symbiosis
848 by phosphate in pea involves early and systemic signalling events. Journal of Experimental Botany. 2011;62:
849 1049–1060. doi:10.1093/jxb/erq335

850 69. Schiessl K, Lilley JLS, Lee T, Tamvakis I, Kohlen W, Bailey PC, et al. NODULE INCEPTION recruits the
851 lateral root developmental program for symbiotic nodule organogenesis in *Medicago truncatula*. Current
852 Biology. 2019;29: 3657-3668.e5. doi:10.1016/j.cub.2019.09.005

853 70. Lefebvre B, Klaus-Heisen D, Pietraszewska-Bogiel A, Hervé C, Camut S, Auriac M-C, et al. Role of N-
854 Glycosylation sites and CXC motifs in trafficking of *Medicago truncatula* Nod Factor perception protein to
855 plasma membrane. J Biol Chem. 2012;287: 10812–10823. doi:10.1074/jbc.M111.281634

856 71. Li J-F, Norville JE, Aach J, McCormack M, Zhang D, Bush J, et al. Multiplex and homologous recombination–
857 mediated genome editing in *Arabidopsis* and *Nicotiana benthamiana* using guide RNA and Cas9. Nat
858 Biotechnol. 2013;31: 688–691. doi:10.1038/nbt.2654

859 72. Brini M, Marsault R, Bastianutto C, Alvarez J, Pozzan T, Rizzuto R. Transfected aequorin in the
860 measurement of cytosolic Ca2+ concentration. Journal of Biological Chemistry. 1995;270: 9896–9903.
861 doi:10.1074/jbc.270.17.9896

862 73. Di Tommaso P, Chatzou M, Floden EW, Barja PP, Palumbo E, Notredame C. Nextflow enables reproducible
863 computational workflows. Nat Biotechnol. 2017;35: 316–319. doi:10.1038/nbt.3820

74. Ewels PA, Peltzer A, Fillinger S, Patel H, Alneberg J, Wilm A, et al. The nf-core framework for community-curated bioinformatics pipelines. Nat Biotechnol. 2020;38: 276–278. doi:10.1038/s41587-020-0439-x

75. Krueger F, James F, Ewels P, Afyounian E, Schuster-Boeckler B. FelixKrueger/TrimGalore: v0.6.7 - DOI via Zenodo. Zenodo; 2021. doi:10.5281/zenodo.5127899

76. Kopylova E, Noé L, Touzet H. SortMeRNA: fast and accurate filtering of ribosomal RNAs in metatranscriptomic data. Bioinformatics. 2012;28: 3211–3217. doi:10.1093/bioinformatics/bts611

77. Quinlan AR, Hall IM. BEDTools: a flexible suite of utilities for comparing genomic features. Bioinformatics. 2010;26: 841–842. doi:10.1093/bioinformatics/btq033

78. Team RC. R: A language and environment for statistical computing. MSOR connections. 2014;1. Available: https://api.semanticscholar.org/CorpusID:215755663

79. Love MI, Huber W, Anders S. Moderated estimation of fold change and dispersion for RNA-seq data with DESeq2. Genome Biology. 2014;15: 550. doi:10.1186/s13059-014-0550-8

80. Sayols S, Scherzinger D, Klein H. dupRadar: a Bioconductor package for the assessment of PCR artifacts in RNA-Seq data. BMC Bioinformatics. 2016;17: 428. doi:10.1186/s12859-016-1276-2

81. Andrews S. FastQC: a quality control tool for high throughput sequence data. 2010 [cited 15 Nov 2024]. Available: http://www.bioinformatics.babraham.ac.uk/projects/fastqc/

82. Pertea G, Pertea M. GFF Utilities: GffRead and GffCompare. F1000Research. 2020;9: ISCB Comm J. doi:10.12688/f1000research.23297.2

83. Wall L, Christiansen T, Orwant J. Programming perl. O'Reilly Media, Inc.; 2000.

84. Van Rossum G, Drake FL. Python 3 Reference Manual. Scotts Valley, CA: CreateSpace; 2009.

85. Li B, Dewey CN. RSEM: accurate transcript quantification from RNA-Seq data with or without a reference genome. BMC Bioinformatics. 2011;12: 323. doi:10.1186/1471-2105-12-323

86. Dobin A, Davis CA, Schlesinger F, Drenkow J, Zaleski C, Jha S, et al. STAR: ultrafast universal RNA-seq aligner. Bioinformatics. 2013;29: 15–21. doi:10.1093/bioinformatics/bts635

87. Picard toolkit. Broad Institute, GitHub repository. Broad Institute; 2019. Available: https://broadinstitute.github.io/picard/

88. Okonechnikov K, Conesa A, García-Alcalde F. Qualimap 2: advanced multi-sample quality control for high-throughput sequencing data. Bioinformatics. 2016;32: 292–294. doi:10.1093/bioinformatics/btv566

89. Wang L, Wang S, Li W. RSeQC: quality control of RNA-seq experiments. Bioinformatics. 2012;28: 2184–2185. doi:10.1093/bioinformatics/bts356

90. Patro R, Duggal G, Love MI, Irizarry RA, Kingsford C. Salmon provides fast and bias-aware quantification of transcript expression. Nat Methods. 2017;14: 417–419. doi:10.1038/nmeth.4197

91. Morgan M, Obenchain V, Hester J, Pagès H. Summarized Experiment: A container (S4 class) for matrix-like assays. Bioconductor. 2024 [cited 15 Nov 2024]. doi:10.18129/B9.bioc.SummarizedExperiment

92. Danecek P, Bonfield JK, Liddle J, Marshall J, Ohan V, Pollard MO, et al. Twelve years of SAMtools and BCFtools. Gigascience. 2021;10: giab008. doi:10.1093/gigascience/giab008

93. Kovaka S, Zimin AV, Pertea GM, Razaghi R, Salzberg SL, Pertea M. Transcriptome assembly from long-read RNA-seq alignments with StringTie2. Genome Biol. 2019;20: 278. doi:10.1186/s13059-019-1910-1

94. Love MI, Soneson C, Hickey PF, Johnson LK, Pierce NT, Shepherd L, et al. Tximeta: Reference sequence checksums for provenance identification in RNA-seq. PLOS Computational Biology. 2020;16: e1007664. doi:10.1371/journal.pcbi.1007664

95. Wu T, Hu E, Xu S, Chen M, Guo P, Dai Z, et al. clusterProfiler 4.0: A universal enrichment tool for interpreting omics data. Innovation (Camb). 2021;2: 100141. doi:10.1016/j.xinn.2021.100141

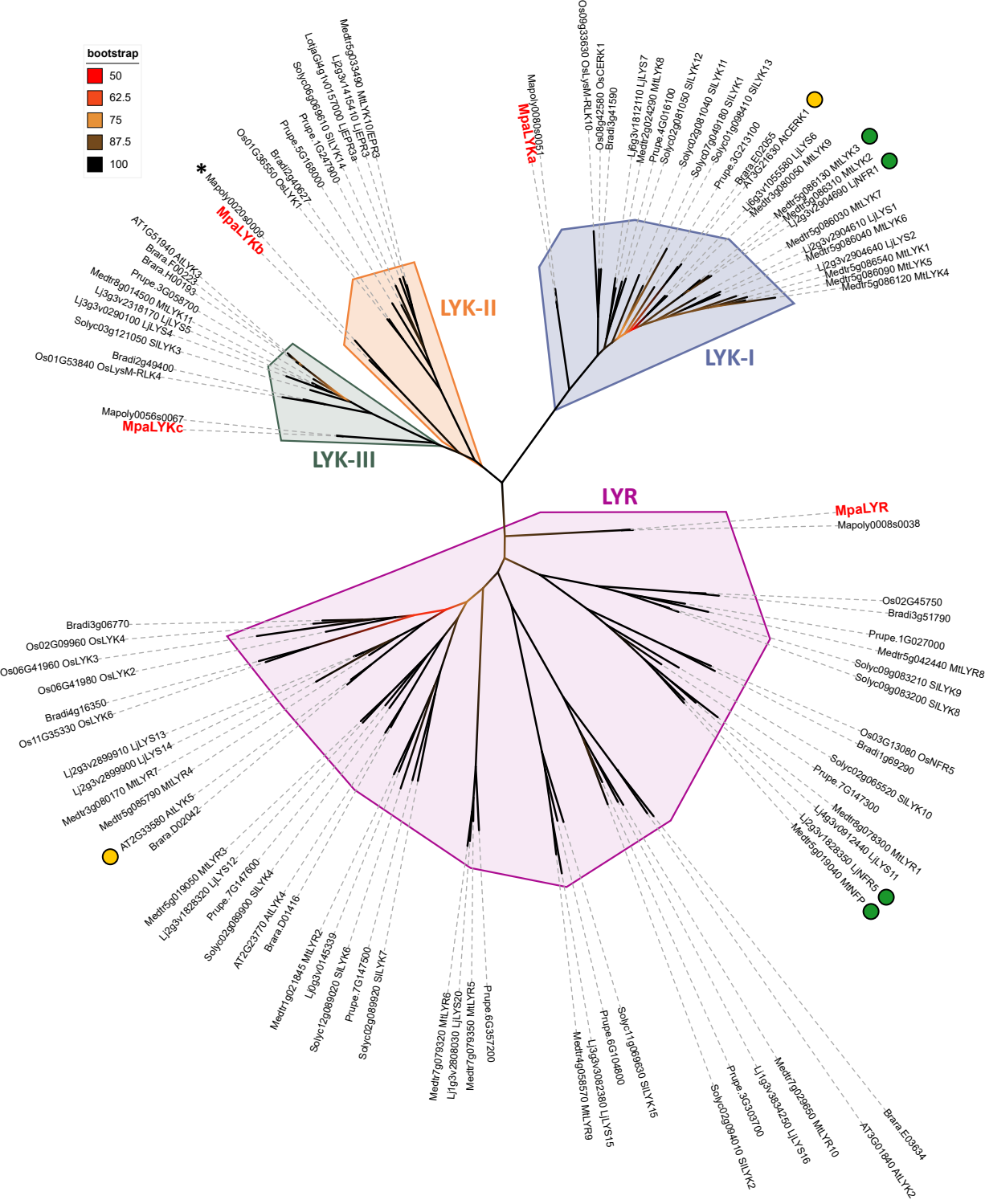
bootstrap
50
62.5
75
87.5
100
LYK-I
LYK-II
LYK-III
LYR
MpaLYKa
MpaLYKb
MpaLYKc
MpaLYR
Mapoly0080s0051
Mapoly0020s0009
Mapoly0056s0067
Mapoly0008s0038
Os09g33630 OsLysM-RLK10
Os08g42580 OsCERK1
Bradi3g41590
Lj6g3v1812110 LjLYS7
Medtr2g024290 MtLYK8
Prupe.4G016100
Solyc02g081050 SlLYK12
Solyc02g081040 SlLYK11
Solyc07g049180 SlLYK1
Solyc01g098410 SlLYK13
Prupe.3G213100
Brara.E02055
AT3G21630 AtCERK1
Lj6g3v1055580 LjLYS6
Medtr3g080050 MtLYK9
Medtr5g086130 MtLYK3
Medtr5g086310 MtLYK2
Lj2g3v2904690 LjNFR1
Medtr5g086030 MtLYK7
Lj2g3v2904610 LjLYS1
Medtr5g086040 MtLYK6
Lj2g3v2904640 LjLYS2
Medtr5g086540 MtLYK1
Medtr5g086090 MtLYK5
Medtr5g086120 MtLYK4
Medtr5g033490 MtLYK10/EPR3
Lj2g3v1415410 LjEPR3
LotjaGi4g1v0157000 LjEPR3a
Solyc06g069610 SlLYK14
Prupe.1G247900
Prupe.5G168000
Bradi2g40627
Os01G36550 OsLYK1
AT1G51940 AtLYK3
Brara.F00223
Brara.H00193
Prupe.3G058700
Medtr8g014500 MtLYK11
Lj3g3v2318170 LjLYS5
Lj3g3v0290100 LjLYS4
Solyc03g121050 SlLYK3
Bradi2g49400
Os01G53840 OsLysM-RLK4
Bradi3g06770
Os02G09960 OsLYK4
Os06G41960 OsLYK3
Os06G41980 OsLYK2
Bradi4g16350
Os11G35330 OsLYK6
Lj2g3v2899910 LjLYS13
Lj2g3v2899900 LjLYS14
Medtr3g080170 MtLYR7
Medtr5g085790 MtLYR4
AT2G33580 AtLYK5
Brara.D02042
Medtr5g019050 MtLYR3
Lj2g3v1828320 LjLYS12
Prupe.7G147600
Solyc02g089900 SlLYK4
AT2G23770 AtLYK4
Brara.D01416
Medtr1g021845 MtLYR2
Lj0g3v0145339
Solyc12g089020 SlLYK6
Prupe.7G147500
Solyc02g089920 SlLYK7
Medtr7g079320 MtLYR6
Lj1g3v2808030 LjLYS20
Medtr7g079350 MtLYR5
Prupe.6G357200
Medtr4g058570 MtLYR9
Lj3g3v3082380 LjLYS15
Prupe.6G104800
Solyc11g069630 SlLYK15
Solyc02g094010 SlLYK2
Prupe.3G303700
Lj1g3v3834250 LjLYS16
Medtr7g029650 MtLYR10
AT3G01840 AtLYK2
Brara.E03634
Os02G45750
Bradi3g51790
Prupe.1G027000
Medtr5g042440 MtLYR8
Solyc09g083210 SlLYK9
Solyc09g083200 SlLYK8
Os03G13080 OsNFR5
Bradi1g69290
Solyc02g065520 SlLYK10
Prupe.7G147300
Medtr8g078300 MtLYR1
Lj4g3v0912440 LjLYS11
Lj2g3v1828350 LjNFR5
Medtr5g019040 MtNFP

Figure 1.

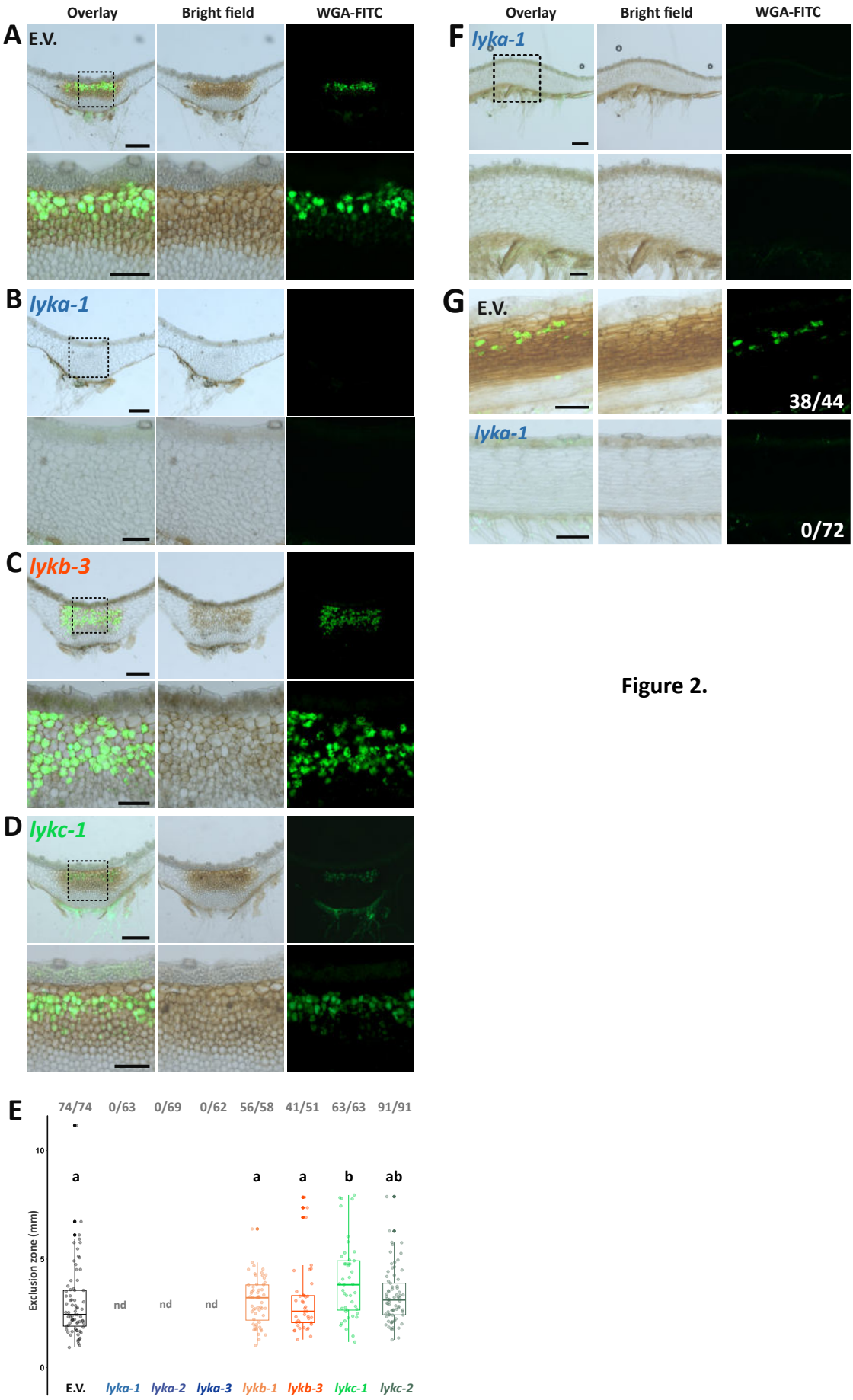
Overlay
Bright field
WGA-FITC
A
E.V.
B
lyka-1
C
lykb-3
D
lykc-1
F
lyka-1
G
E.V.
38/44
lyka-1
0/72
E
74/74
0/63
0/69
0/62
56/58
41/51
63/63
91/91
a
a
a
b
ab
nd
nd
nd
Exclusion zone (mm)
10
5
0
E.V.
lyka-1
lyka-2
lyka-3
lykb-1
lykb-3
lykc-1
lykc-2

Figure 2.

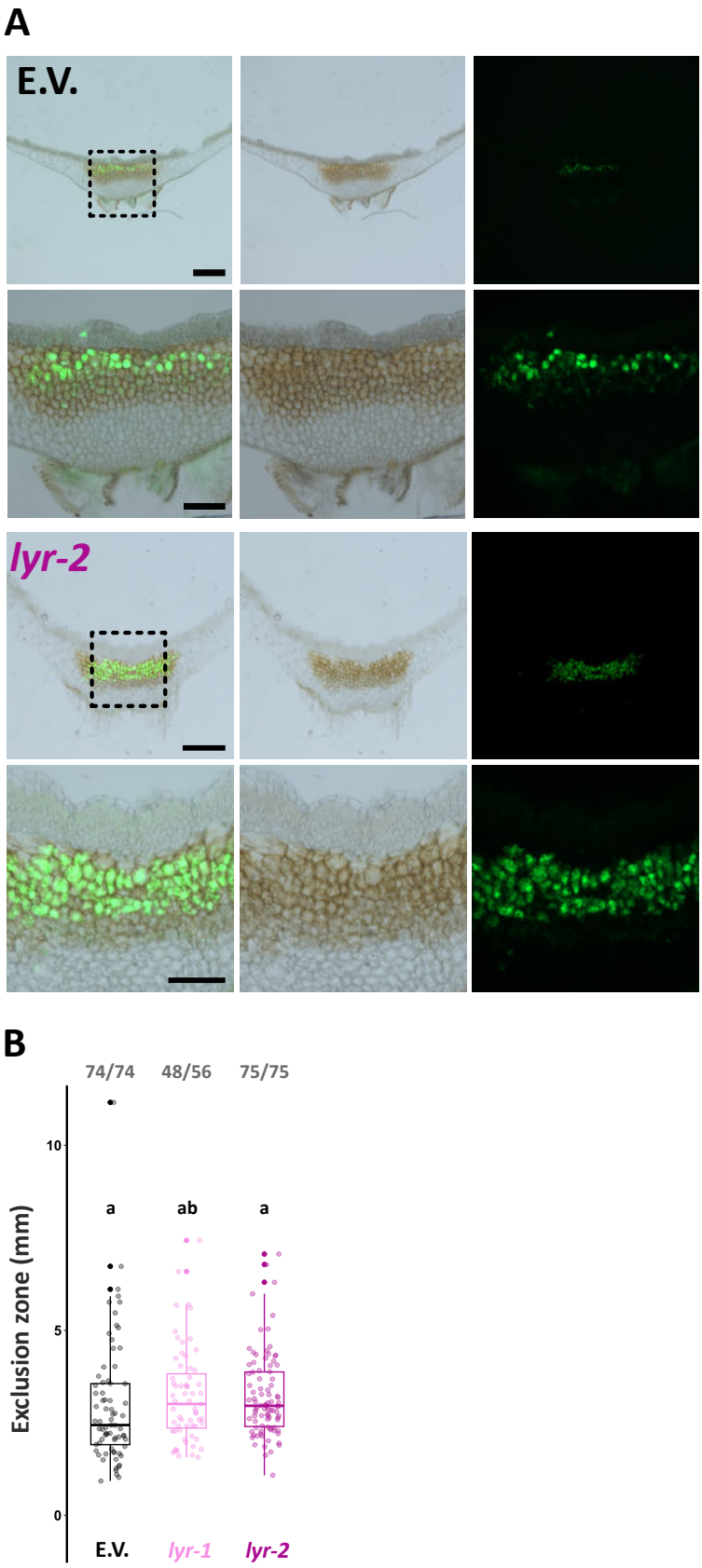
A
E.V.
lyr-2
B
74/74
48/56
75/75
10
5
0
Exclusion zone (mm)
a
ab
a
E.V.
lyr-1
lyr-2

Figure 3.

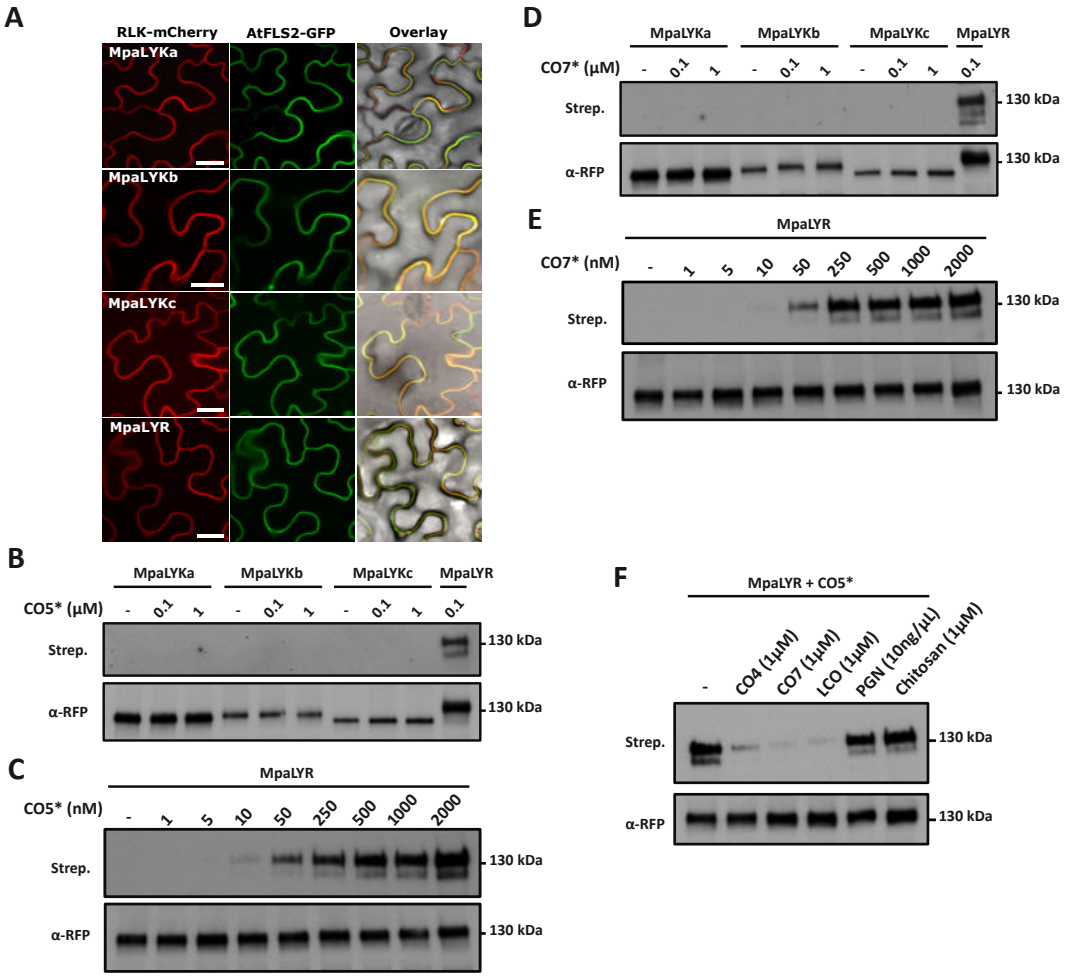
A
RLK-mCherry
AtFLS2-GFP
Overlay
MpaLYKa
MpaLYKb
MpaLYKc
MpaLYR
B
MpaLYKa
MpaLYKb
MpaLYKc
MpaLYR
CO5* (µM)
- 0.1 1 - 0.1 1 - 0.1 1 0.1
Strep.
α-RFP
130 kDa
130 kDa
C
MpaLYR
CO5* (nM)
- 1 5 10 50 250 500 1000 2000
Strep.
α-RFP
130 kDa
130 kDa
D
MpaLYKa
MpaLYKb
MpaLYKc
MpaLYR
CO7* (µM)
- 0.1 1 - 0.1 1 - 0.1 1 0.1
Strep.
α-RFP
130 kDa
130 kDa
E
MpaLYR
CO7* (nM)
- 1 5 10 50 250 500 1000 2000
Strep.
α-RFP
130 kDa
130 kDa
F
MpaLYR + CO5*
- CO4 (1µM) CO7 (1µM) LCO (1µM) PGN (10ng/µL) Chitosan (1µM)
Strep.
α-RFP
130 kDa
130 kDa

Figure 4.

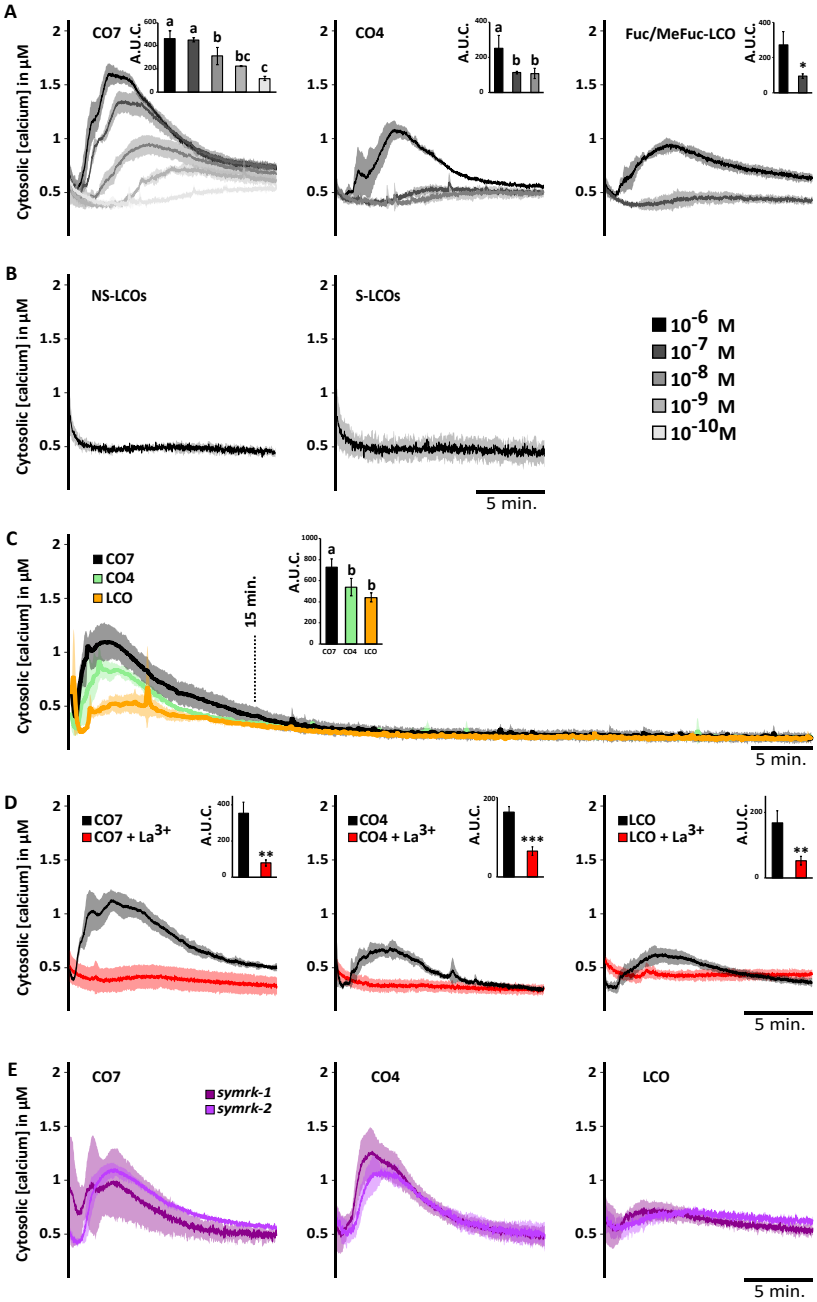
A
CO7
CO4
Fuc/MeFuc-LCO
A.U.C.
Cytosolic [calcium] in µM
B
NS-LCOs
S-LCOs
10^{-6} M
10^{-7} M
10^{-8} M
10^{-9} M
10^{-10}M
5 min.
C
CO7
CO4
LCO
15 min.
5 min.
D
CO7 + La^{3+}
CO4 + La^{3+}
LCO + La^{3+}
5 min.
E
symrk-1
symrk-2
5 min.

Figure 5.

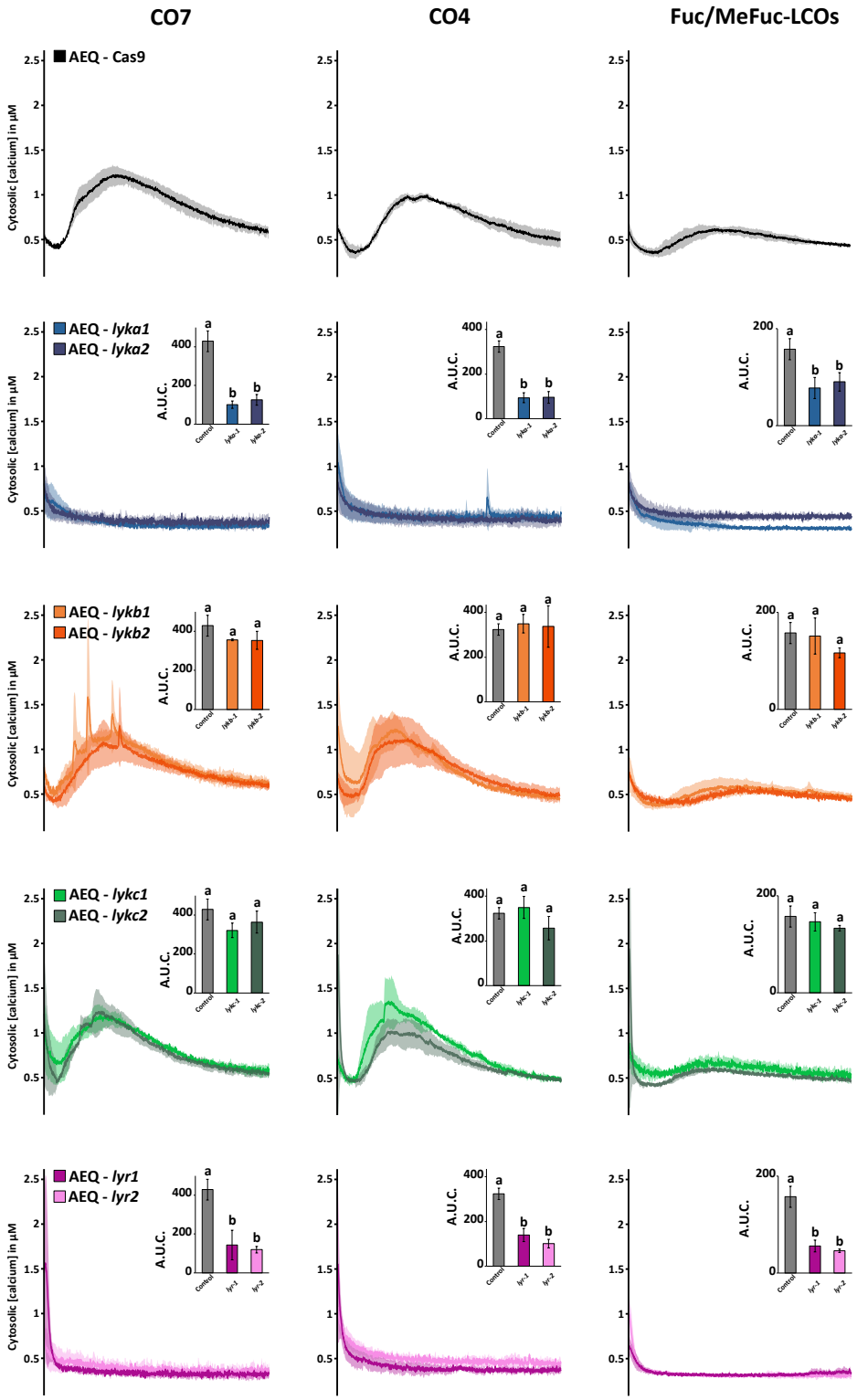
CO7
CO4
Fuc/MeFuc-LCOs
AEQ - Cas9
AEQ - lykα1
AEQ - lykα2
AEQ - lykb1
AEQ - lykb2
AEQ - lykc1
AEQ - lykc2
AEQ - lyr1
AEQ - lyr2
Cytosolic [calcium] in µM
A.U.C.
Control

Figure 6.

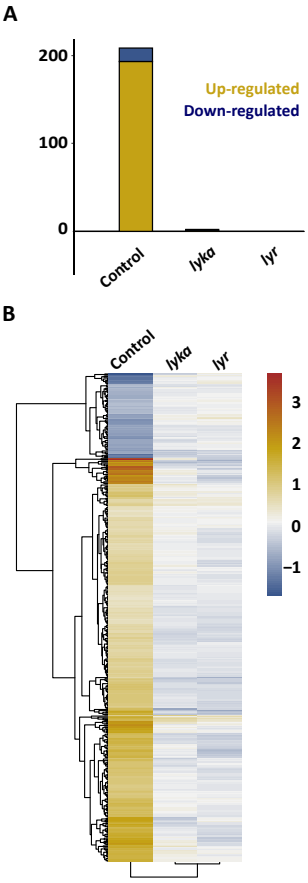
A
200
100
0
Up-regulated
Down-regulated
Control
lyka
lyr
B
Control
lyka
lyr
3
2
1
0
−1

Figure 7.

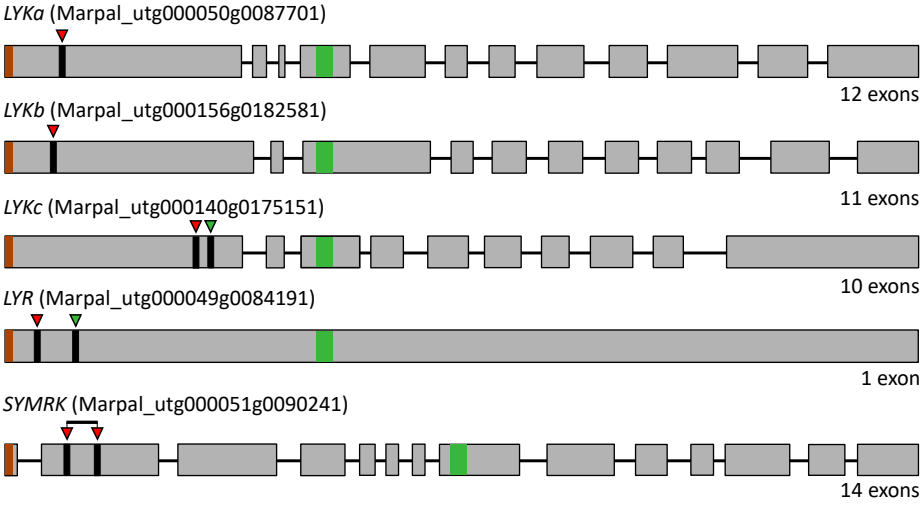

Supplementary Figure 1.

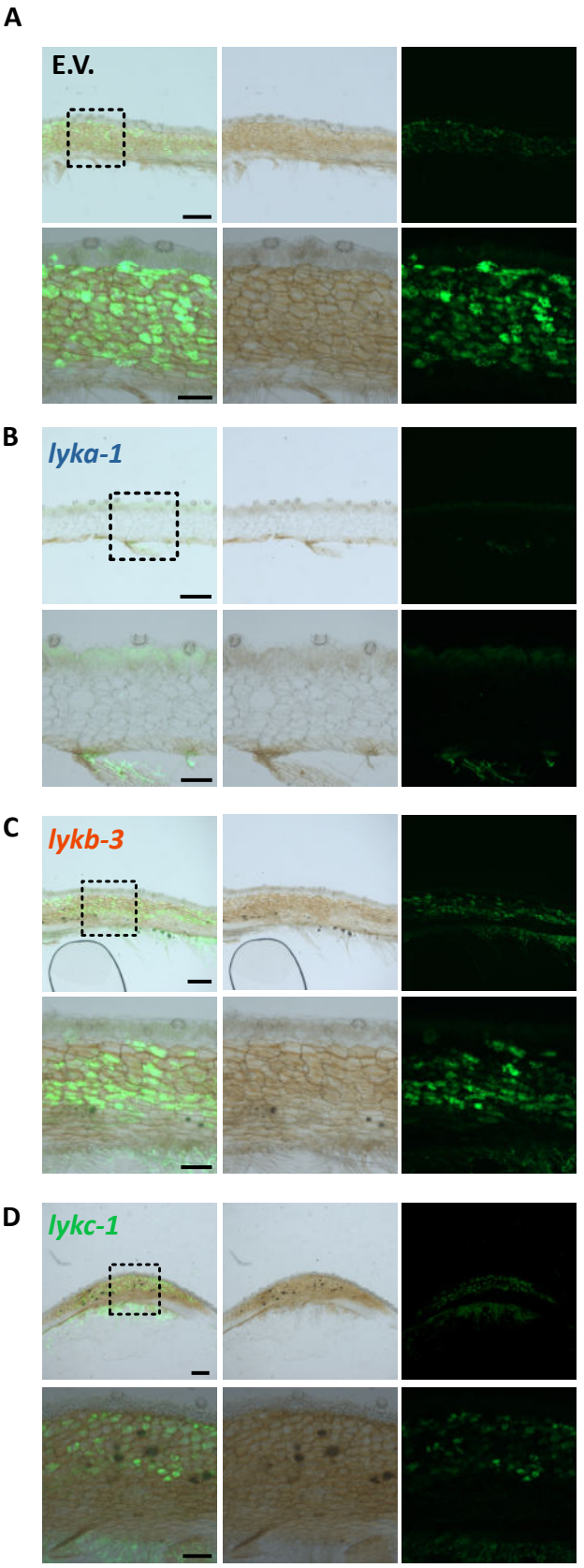

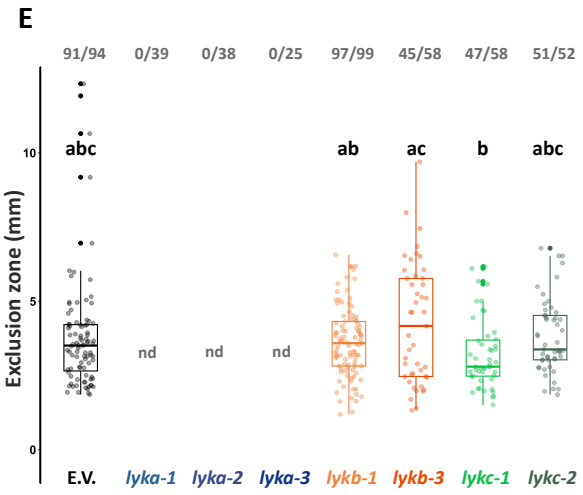

Supplementary Figure 2.

A

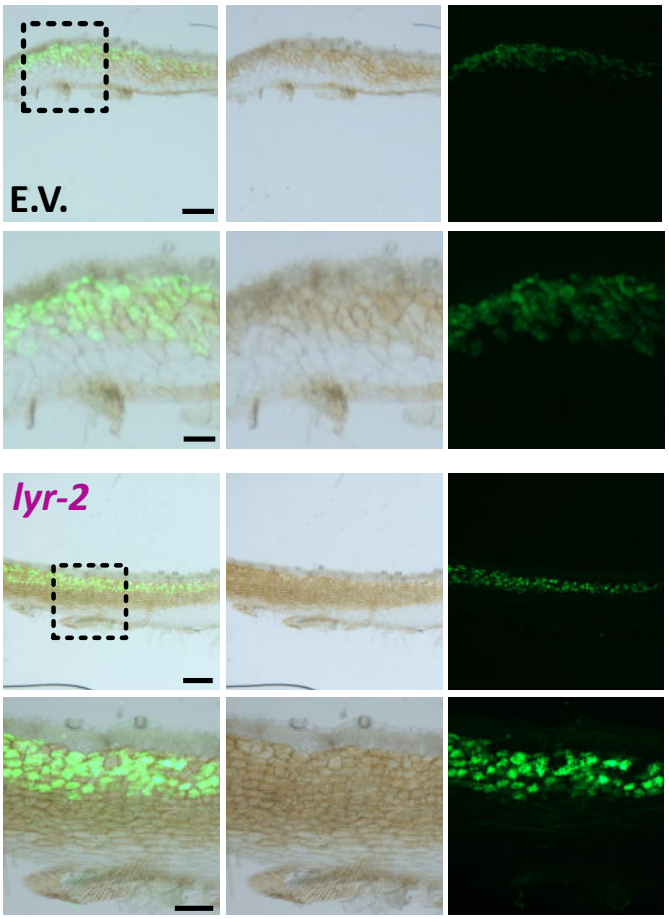

B

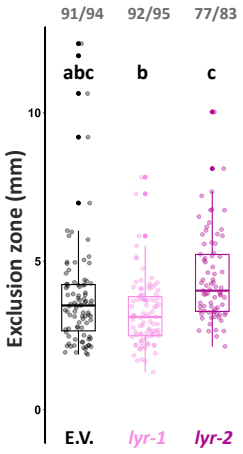

Supplementary Figure 3.

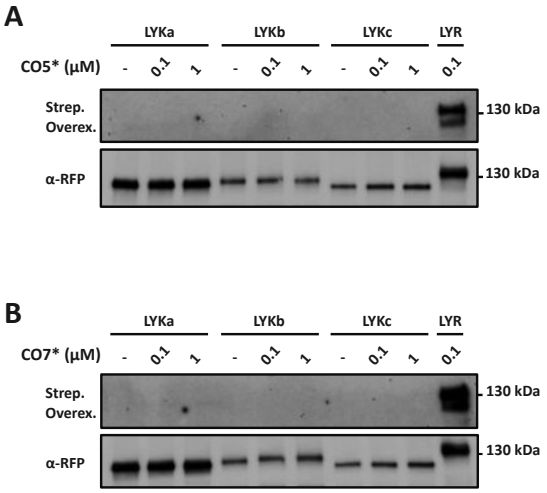

Supplementary Figure 4.

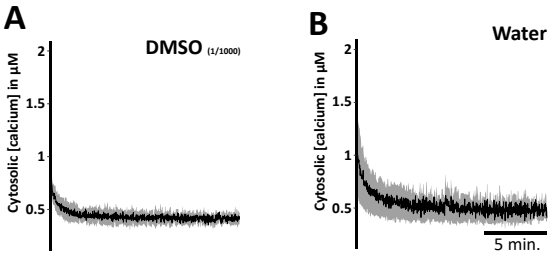

Supplementary Figure 5.

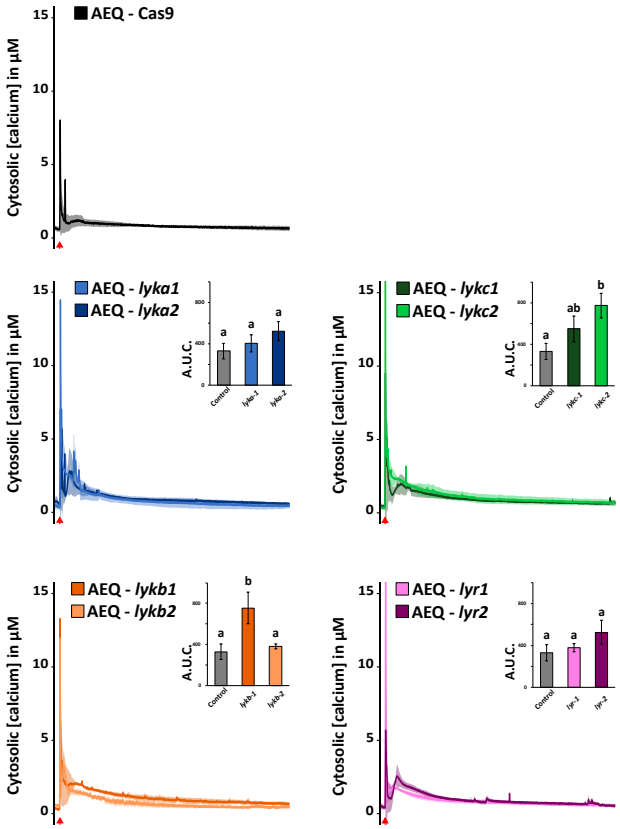

Supplementary Figure 6.

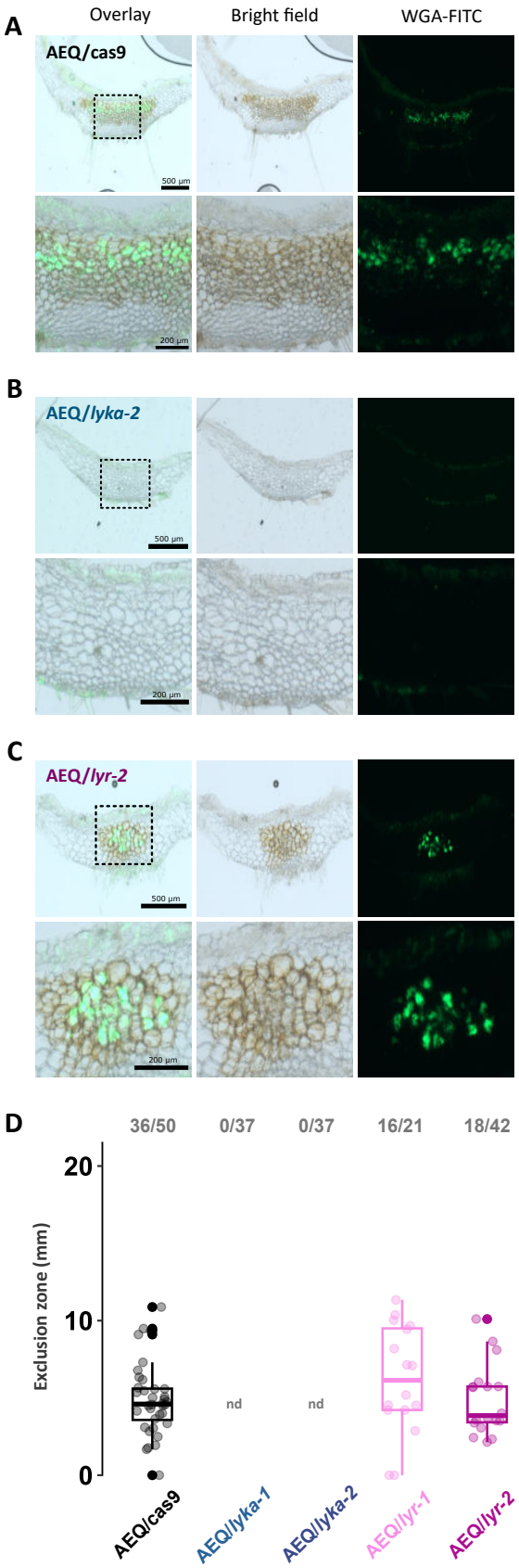

Supplementary Figure 7.

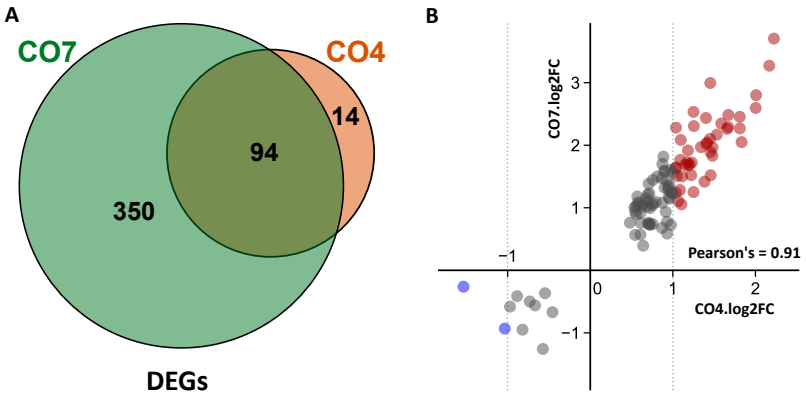

Supplementary Figure 8.

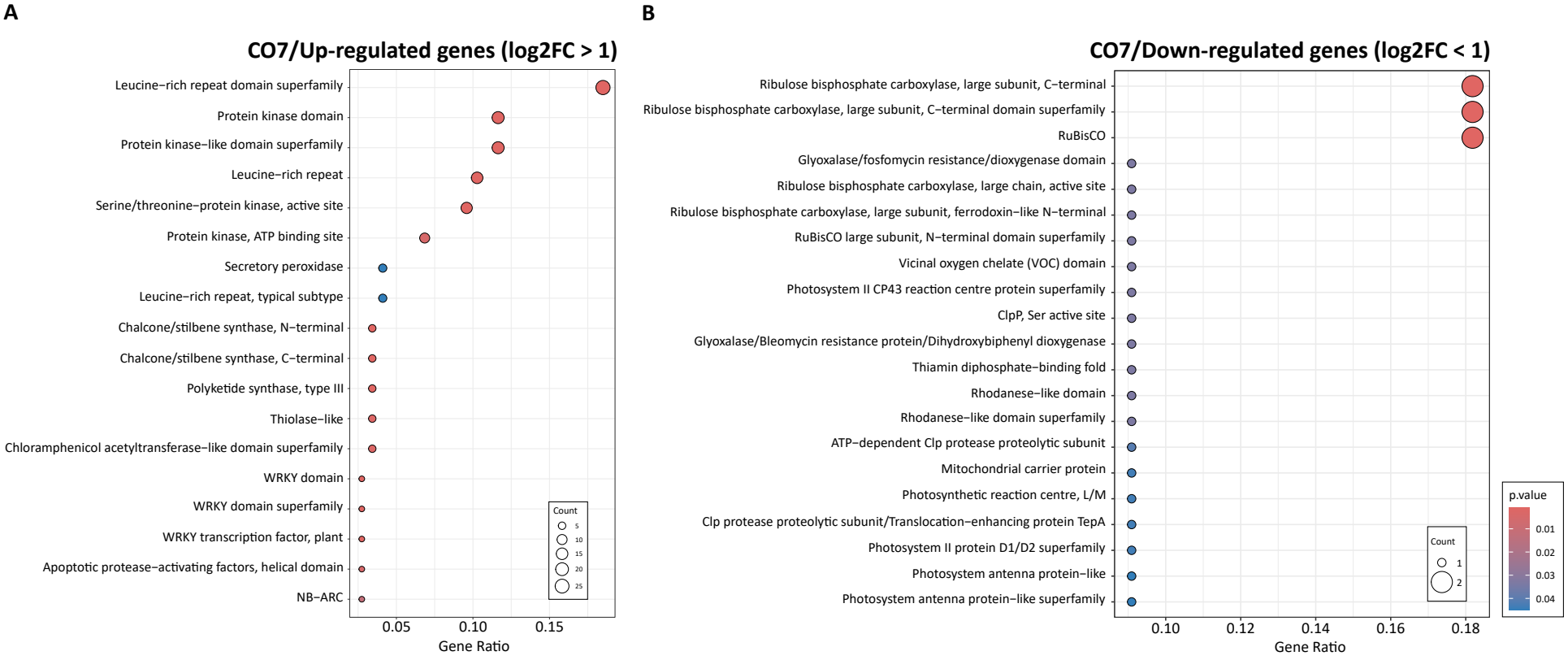

Supplementary Figure 9.

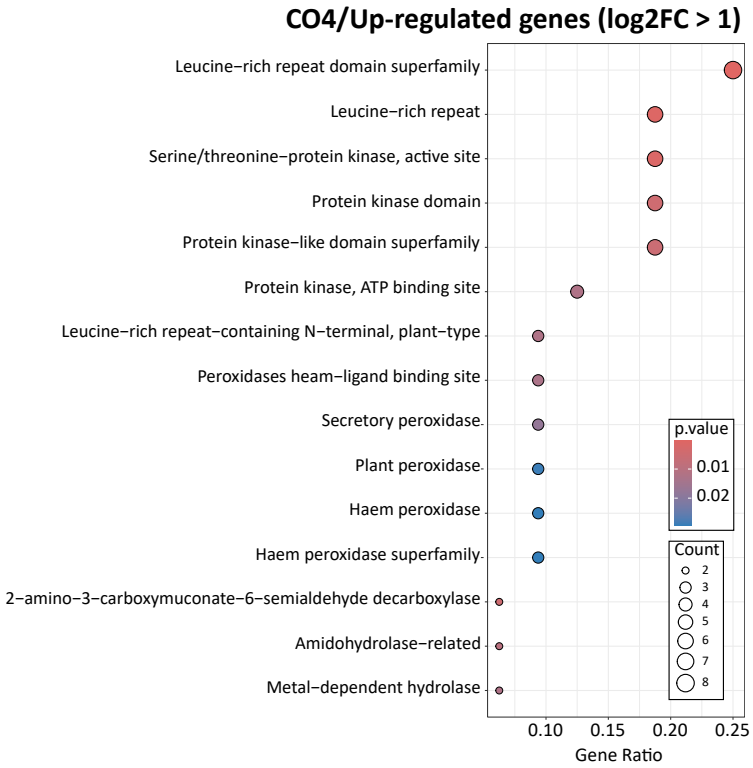

Supplementary Figure 10.

S1 Table. List of protospacers sequences used for gene editions.

	Gene	Protospacer #1	Protospacer #2	Mutant	Mutation
Protospacers sequences (w/o PAM)	Marpal_utg000050g0087701	TGATACTCTCCTAGCTCTGG	-	*lyka-1*	A insertion/frameshift at AA57 leading to STOP
				lyka-2	A insertion/frameshift at AA57 leading to STOP
				lyka-3	A insertion/frameshift at AA57 leading to STOP
	Marpal_utg000156g0182581	CGGAGCGGATTAATCAACTG	-	*lykb-1*	T insertion/frameshift A27 leading to STOP
				lykb-2	19bp deletion/frameshit AA27 leading to STOP
	Marpal_utg000140g0175151	GGACCGTTACGATGCGGATA	-	*lykc-1*	T insertion/frameshift at AA180 leading to STOP
		-	GCTCGGGAAGTAGCTGACAT	*lykc-2*	G insertion/frameshift at AA192 leading to STOP
	Marpal_utg000049g0084191	ACTCGTGCTCAACAGGTCTA	-	*lyr-1*	T insertion/frameshift at AA26 leading to STOP
		-	TTACAAAGACATTCCCGCTG	*lyr-2*	A insertion/frameshift at AA61 leading to STOP
	Marpal_utg000050g0087701	TGATACTCTCCTAGCTCTGG	-	*AEQ-lyka-1*	T insertion/frameshit AA57 leading to STOP
				AEQ-lyka-2	T insertion/frameshit AA57 leading to STOP
	Marpal_utg000156g0182581	CGGAGCGGATTAATCAACTG	-	*AEQ-lykb-1*	T insertion/frameshift at AA27 leading to STOP
				AEQ-lykb-2	T insertion/frameshift at AA27 leading to STOP
	Marpal_utg000140g0175151	GGACCGTTACGATGCGGATA	-	*AEQ-lykc-1*	7pb insertion/frameshift at AA179 leading to STOP
				AEQ-lykc-2	G insertion/frameshift at AA179 leading to STOP
	Marpal_utg000049g0084191	ACTCGTGCTCAACAGGTCTA	-	*AEQ-lyr-1*	T insertion/frameshift at AA26 leading to STOP
				AEQ-lyr-2	T insertion/frameshift at AA26 leading to STOP
	Marpal_utg000051g0090241	CGGGATCAGATTTAAGCCTG	TAGCGTATAAAAAGGTCCCG	*AEQ-symrk-1*	80bp deletion/frameshift at AA81 leading to STOP
				AEQ-symrk-2	80bp deletion/frameshift at AA81 leading to STOP

S2 Table. List of differentially regulated genes in response to CO7 and CO4 in *M. paleacea* WT and CO7 for *lyka* and *lyr*.

Not provided

S3 Table. InterPro terms enrichment analyses in response to CO7 and CO4.

Not provided

S4 Table. List of primers for genotyping edited lines.

	Gene codes	Primer #1	Primer #2	Target gene
Primers for gRNA cloning	Marpal_utg000050g0087701_ g1	TCTCGTGATACTCTCCTAGCTCTGG	AAACCCAGAGCTAGGAGAGTATCAC	LYKa
	Marpal_utg000156g0182581_g1	TCTCGCGGAGCGGATTAATCAACTG	AAACCAGTTGATTAATCCGCTCCGC	LYKb
	Marpal_utg000140g0175151_g1	TCTCGGGACCGTTACGATGCGGATA	AAACTATCCGCATCGTAACGGTCCC	LYKc
	Marpal_utg000140g0175151_g2	TCTCGGCTCGGGAAGTAGCTGACAT	AAACATGTCAGCTACTTCCCGAGCC	LYKc
	Marpal_utg000049g0084191_g1	TCTCGACTCGTGCTCAACAGGTCTA	AAACTAGACCTGTTGAGCACGAGTC	LYR
	Marpal_utg000049g0084191_g2	TCTCGTTACAAAGACATTCCCGCTG	AAACCAGCGGGAATGTCTTTGTAAC	LYR
Genotyping primers	Marpal_utg000050g0087701	TGAGAATTCGCCTGTAGTTTG	ACCTTTCTGGGGGATAAAGATGA	LYKa
	Marpal_utg000156g0182581	ATGAGAGCGAGGAGTCCCGTA	GAAGTTGAGCGGGATGAAGAGGT	LYKb
	Marpal_utg000140g0175151	GTTTCAGACATCATGGAACAAAAAG	CCGTTCAACCGATCATAGTAC	LYKc
	Marpal_utg000049g0084191	AGGTGATTTCAAAGTGGGAGAC	TCCAGAGTGTTGTTGCTGAG	LYR
	Marpal_utg000051g0090241	AATGGAGGACACAGGAGAAGC	AACCCAAGACAAAACCAGTAAGG	SYMRK

S5 Table. List of constructs and selected lines used in this study.

CONSTRUCT	SOURCE	IDENTIFIER
BIOLOGICAL SAMPLES		
Marchantia paleacea empty control 132.2	Rich et *al.* 2021	N/A
M. paleacea (lyka)	This paper	N/A
M. paleacea (lykb)	This paper	N/A
M. paleacea (lykc)	This paper	N/A
M. paleacea (lyr)	This paper	N/A
M. paleacea (AEQ-Cas9)	This paper	N/A
M. paleacea (AEQ-lyka)	This paper	N/A
M. paleacea (AEQ-lykb)	This paper	N/A
M. paleacea (AEQ-lykc)	This paper	N/A
M. paleacea (AEQ-lyr)	This paper	N/A
M. paleacea (AEQ-symrk)	This paper	N/A
RECOMBINANT DNA		
pUPD2 - AEQUORIN (B3-B5) (L0)	This paper	N/A
pMS - MpalLYKa (L0)	This paper	N/A
pMS - MpalLYKb (L0)	This paper	N/A
pMS - MpalLYKc (L0)	This paper	N/A
pMS - MpalLYR (L0)	This paper	N/A
C-terminal mCherry (L0)	Addgene	pICSL50004
pro35S - short (L0)	Addgene	pICH51277
proAtUBQ10 (L0)	This paper	N/A
35Ster (L0)	Addgene	pICH41414
Noster (L0)	Addgene	pICH41421
pL1F2 - proAtUBI10::MpalLYKA-mcherry-35Ster (L1)	This paper	N/A
pL1F2 - proAtUBI10::MpaLYKB-mcherry-35Ster (L1)	This paper	N/A
pL1F2 - proAtUBI10::MpaLYKC-mcherry-35Ster (L1)	This paper	N/A
pL1F2 - proAtUBI10::MpaLYR-mcherry-35Ster (L1)	This paper	N/A
pL1R1 - pro35S::HygroR-Noster (L1)	ENSA	EC15030
L1-R1 - p35S-ChlorosulfuronR_V2-35Ster	ENSA	1PMD1030
pL1F2 - proMpolEF1a::AEQUORIN-Noster (L1)	This paper	N/A
pL1-R2 - pMpaEF1a:AtCas9:NLS-35Ster (L1)	ENSA	1PMD527
pL1-R3 - pMpoU6-1:sgRNA-tRNAP (L1)	Rich et *al.* 2021	1PMD97
pL2b - Hygro-MpalLYKa_guide1 (L2)	This paper	N/A
pL2b - Hygro-MpalLYKb_guide1 (L2)	This paper	N/A
pL2b - Hygro-MpalLYKc_guide1 (L2)	This paper	N/A
pL2b - Hygro-MpalLYKc_guide2 (L2)	This paper	N/A
pL2b - Hygro-MpalLYR_guide1 (L2)	This paper	N/A
pL2b - Hygro-MpalLYR_guide2 (L2)	This paper	N/A
pL2b - Chlorosulfuron-MpalLYKa_guide1 (L2)	This paper	N/A
pL2b - Chlorosulfuron-MpalLYKb_guide1 (L2)	This paper	N/A
pL2b - Chlorosulfuron-MpalLYKc_guide1 (L2)	This paper	N/A
pL2b - Chlorosulfuron-MpalLYR_guide1 (L2)	This paper	N/A
pL2b - Chlorosulfuron-MpalSYMRK_guide1&2 (L2)	This paper	N/A
pL2b - HygroR - proMpolEF1a::AEQUORIN-Noster (L2)	This paper	N/A
pAtFLS2::AtFLS2–3xmyc-GFP-35Ster	Robatzek et al., 2006	N/A